DEVELOPMENT OF ANALYTICAL SOLUTION FOR THERMO-MECHANICAL STRESSES OF MULTILAYERED PRESSURE VESSEL BASED ON RECURSIVE ALGORITHM

SIM LIH CHI

MASTER OF ENGINEERING SCIENCE

LEE KONG CHIAN FACULTY OF ENGINEERING AND SCIENCE
UNIVERSITI TUNKU ABDUL RAHMAN
JANUARY 2022

DEVELOPMENT OF ANALYTICAL SOLUTION FOR THERMO-MECHANICAL STRESSES OF MULTILAYERED PRESSURE VESSEL BASED ON RECURSIVE ALGORITHM

By

SIM LIH CHI

A dissertation submitted to
Lee Kong Chian Faculty of Engineering and Science,
Universiti Tunku Abdul Rahman,
in partial fulfillment of the requirements for the degree of
Master of Engineering Science in
January 2022

ABSTRACT

DEVELOPMENT OF ANALYTICAL SOLUTION FOR THERMO-MECHANICAL STRESSES OF MULTILAYERED PRESSURE VESSEL BASED ON RECURSIVE ALGORITHM

Sim Lih Chi

Multilayered pressure vessel is commonly used under harsh conditions, particularly in high pressure and high temperature environment. Thus, the evaluation of the stresses induced within the multilayered pressure vessel's wall is crucial to ensure safe operation. Recent studies showed that analytical solution based on recursive algorithm can be used to obtain thermo-mechanical stresses of multilayered structure efficiently. However, there is no study has been conducted for the derivation of analytical solutions for multilayered spherical pressure vessel and cylindrical pressure vessel under generalized plane strain condition. Hence, the present work aimed to derive the analytical solution by using recursive algorithm for multilayered cylindrical and spherical pressure vessels which are subjected to thermo-mechanical loading. Firstly, the analytical solution for temperature distribution across the multilayered vessel wall was derived. Next, the analytical solutions for radial, tangential and axial stresses distribution across the multilayered vessel wall were derived. After that, verification was carried out on the proposed analytical solutions by using two finite element analysis models reported in literatures. The simulated results were in good agreement with the output from the proposed analytical solutions. In addition, the validated analytical solutions were demonstrated as the

alternative method to analyze the stresses of functionally graded material (FGM) cylindrical and spherical pressure vessel under thermo-mechanical loading. In general, the stresses results obtained based on present proposed analytical solutions were compared with the FGM exact solution reported in literatures and the overall percentage of difference is less than 1%.

ACKNOWLEDGEMENT

I would like to express my deepest appreciation to everyone who have assisted me in this study. The completion of the research would not have been possible without the help from others. First and foremost, I would like to thank Asst. Prof. Ts. Dr. Yeo Wei Hong for his immeasurable support and guidance throughout the whole journey. Dr. Yeo has been a responsible and enthusiastic supervisor. Despite this period of pandemic, he has been very responsive towards my doubts and questions. From time to time, Dr. Yeo would actively keep track of my progress to make sure things can be accomplished in a timely manner. Other than that, Dr. Yeo's research experience and strong knowledge on the research subject have given me confidence throughout the research.

Also, I am very grateful to have Assoc. Prof. Ir. Ts. Dr. Bernard Saw Lip Huat as my co-supervisor. His valuable feedbacks and comments have helped to improve my work's quality. Last but not least, I would like to thank my family members for their tolerance, physical and mental support during my studies.

APPROVAL SHEET

This dissertation entitled **"DEVELOPMENT OF ANALYTICAL SOLUTION FOR THERMO-MECHANICAL STRESSES OF MULTILAYERED PRESSURE VESSEL BASED ON RECURSIVE ALGORITHM"** was prepared by SIM LIH CHI and submitted as partial fulfillment of the requirements for the degree of Master of Engineering Science at Universiti Tunku Abdul Rahman.

Approved by:

Ts. Dr. Yeo Wei Hong
Assistant Professor/ Head
Department of Mechanical and Material Engineering
Lee Kong Chian Faculty of Engineering and Science
Universiti Tunku Abdul Rahman

04-Jan-22

_____
(Asst. Prof. Ts. Dr. YEO WEI HONG)
Date:……..
Supervisor
Department of Mechanical and Material Engineering
Lee Kong Chian Faculty of Engineering and Science
Universiti Tunku Abdul Rahman

bernard saw
_____
(Assoc. Prof. Ir. Ts. Dr. BERNARD SAW LIP HUAT)
Date: 4/1/2021……..
Co-supervisor
Department of Mechanical and Material Engineering
Lee Kong Chian Faculty of Engineering and Science
Universiti Tunku Abdul Rahman

LEE KONG CHIAN FACULTY OF ENGINEERING AND SCIENCE

UNIVERSITI TUNKU ABDUL RAHMAN

Date: 04-Jan-2022

SUBMISSION OF DISSERTATION

It is hereby certified that **SIM LIH CHI** (ID No: **18UEM07359**) has completed this dissertation entitled **"DEVELOPMENT OF ANALYTICAL SOLUTION FOR THERMO-MECHANICAL STRESSES OF MULTILAYERED PRESSURE VESSEL BASED ON RECURSIVE ALGORITHM"** under the supervision of **Asst. Prof. Ts. Dr. YEO WEI HONG** (Supervisor) from the Department of Mechanical and Material Engineering, Lee Kong Chian Faculty of Engineering and Science, and **Assoc. Prof. Ir. Ts. Dr. BERNARD SAW LIP HUAT** (Co-Supervisor) from the Department of Mechanical and Material Engineering, Lee Kong Chian Faculty of Engineering and Science.

I understand that University will upload softcopy of my dissertation in pdf format into UTAR Institutional Repository, which may be made accessible to UTAR community and public.

Yours truly,

(Sim Lih Chi)

DECLARATION

I hereby declare that the dissertation is based on my original work except for quotations and citations which have been duly acknowledged. I also declare that it has not been previously or concurrently submitted for any other degree at UTAR or other institutions.

Name Sim Lih Chi

Date 04-Jan-2022

TABLE OF CONTENTS

LIST OF TABLES

LIST OF FIGURES

LIST OF FIGURES

LIST OF ABBREVIATIONS

ASME	American Society of Mechanical Engineers
FEM	Finite Element Method
FGM	Functionally Graded Material
$\boldsymbol{E_i}$	Elastic modulus for *i*-th layer $[Pa]$
$\boldsymbol{\nu_i}$	Poisson's ratio for *i*-th layer [-]
$\boldsymbol{\alpha_i}$	Thermal expansion coefficient for *i*-th layer $[°C^{-1}]$
$\boldsymbol{k_i}$	Thermal conductivity for *i*-th layer $[Wm^{-1}°C^{-1}]$
$\boldsymbol{r_i}$	Outer radius for *i*-th layer $[m]$
$\boldsymbol{r}$	Radial coordinate $[m]$
$\boldsymbol{r_0}$	Inner radius for first layer $[m]$
$\boldsymbol{r_n}$	Outer radius for outermost layer $[m]$
$\boldsymbol{P_{int}}$	Pressure loading at inner surface of vessel $[Pa]$
$\boldsymbol{P_{ext}}$	Pressure loading at outer surface of vessel $[Pa]$
$\boldsymbol{\overline{T}_{int}}$	Temperature at inner surface of vessel [°C]
$\boldsymbol{\overline{T}_{ext}}$	Temperature at outer surface of vessel [°C]
$\boldsymbol{\overline{T}_i}$	Temperature at surface/interface points [°C]
$\boldsymbol{T_i}$	Temperature distribution for *i*-th layer [°C]
$\boldsymbol{q''_i}$	Radial heat flux for *i*-th layer $[Wm^{-2}]$
$\boldsymbol{u_{r,i}}$	Radial displacement for *i*-th layer $[m]$
$\boldsymbol{A_i}$	Integration constant for *i*-th layer Defined by Eq. (3.25) [°C] for cylinder Defined by Eq. (3.97) [°C] for sphere
$\boldsymbol{B_i}$	Integration constant for *i*-th layer Defined by Eq. (3.26) [°C] for cylinder Defined by Eq. (3.98) [m°C] for sphere

LIST OF ABBREVIATIONS

$\boldsymbol{x_i}$	$= \delta_i \delta_{i+1}$ [-] for cylinder $= (1/r_i)[(k_i/k_{i+1}) - 1] - (1/r_{i+1})(k_i/k_{i+1})$ $[\ m^{-1}\ ]$ for sphere
$\boldsymbol{y_i}$	$= \delta_{i+1} - (k_i/k_{i+1})(\delta_{i+1} - 1)$ [-] for cylinder $= 1/r_{i-1}$ $[m^{-1}]$ for sphere
$\boldsymbol{\delta_i}$	$= \ln r_{i-1}/\ln r_i$ [-] for cylinder
$\boldsymbol{a_i}$	Recursive relation Defined by Eq. (3.27) [-] for cylinder Defined by Eq. (3.99) [-] for sphere
$\boldsymbol{b_i}$	Recursive relation Defined by Eq. (3.28) [-] for cylinder Defined by Eq. (3.100) [-] for sphere
$\emptyset$	Azimuthal angle coordinate
$\boldsymbol{z}$	Axial coordinate [m]
$\boldsymbol{\theta}$	Polar angle coordinate
$\boldsymbol{\epsilon_{rr,i}}$	Radial strain for *i*-th layer [-]
$\boldsymbol{\epsilon_{\emptyset\emptyset,i}}$	Tangential strain in azimuthal angle direction for *i*-th layer [-]
$\boldsymbol{u_{z,i}}$	Axial displacement for *i*-th layer $[m]$ for cylinder
$\boldsymbol{\epsilon_{zz,i}}$	Axial strain for *i*-th layer [-] for cylinder
$\boldsymbol{\epsilon_{\theta\theta,i}}$	Tangential strain in polar angle direction for *i*-th layer [-] for sphere
$\boldsymbol{\sigma_{rr,i}}$	Radial stress distribution for *i*-th layer $[Pa]$
$\boldsymbol{\sigma_{\emptyset\emptyset,i}}$	Tangential stress distribution in azimuthal angle direction for *i*-th layer $[Pa]$
$\boldsymbol{\sigma_{zz,i}}$	Axial stress distribution for *i*-th layer $[Pa]$ for cylinder

LIST OF ABBREVIATIONS

$\boldsymbol{\sigma_{\theta\theta,i}}$	Tangential stress distribution in polar angle direction for *i*-th layer $[Pa]$ for sphere
$\boldsymbol{I_i}$	$= -[E_i\alpha_i/(1-\nu_i)]\int_{r_{i-1}}^{r}\Delta_i r dr$ $[m^2Pa]$ for cylinder $= \int_{r_{i-1}}^{r}\Delta_i r^2 dr$ $[m^3°C]$ for sphere
$\boldsymbol{\beta_i}$	$= (1+\nu_i)(1-2\nu_i)/E_i$ $[Pa^{-1}]$ for cylinder $= (1-2\nu_i)/E_i$ $[Pa^{-1}]$ for sphere
$\boldsymbol{\lambda_i}$	$= -(1+\nu_i)/E_i$ $[Pa^{-1}]$ for cylinder $= -(1+\nu_i)/2E_i$ $[Pa^{-1}]$ for sphere
$\boldsymbol{\widehat{C}_i}$	Integration constant for *i*-th layer
$\boldsymbol{\widehat{D}_i}$	Integration constant for *i*-th layer
$\boldsymbol{C_i}$	$= \boldsymbol{\widehat{C}_i/\beta_i}$ Defined by Eq. (3.64) $[Pa]$ for cylinder Defined by Eq. (3.135) $[Pa]$ for sphere
$\boldsymbol{D_i}$	$= \boldsymbol{\widehat{D}_i/\lambda_i}$ Defined by Eq. (3.63) $[m^2Pa]$ for cylinder Defined by Eq. (3.134) $[m^3Pa]$ for sphere
$\boldsymbol{\varphi_i}$	$= \boldsymbol{\nu_i\epsilon_{zz}/\beta_i}$ $[Pa]$ for cylinder $= -\boldsymbol{(1-\nu_i)/2E_i\alpha_i}$ $[Pa^{-1}°C]$ for sphere
$\boldsymbol{p_i}$	Radial contact pressure at surface/interface points $[Pa]$
$\boldsymbol{\gamma_i}$	$= r_{i-1}^2/r_i^2$ [-] for cylinder $= r_{i-1}^3/r_i^3$ [-] for sphere
$\boldsymbol{S_i}$	$= \gamma_i\gamma_{i+1}(\lambda_i-\beta_{i+1}) + (\lambda_{i+1}-\lambda_i)\gamma_i$ $[Pa^{-1}]$
$\boldsymbol{G_i}$	$= \lambda_{i+1} - \beta_i + (\beta_i-\beta_{i+1})\gamma_{i+1}$ $[Pa^{-1}]$
$\boldsymbol{c_i}$	Recursive relation Defined by Eq. (3.65) [-] for cylinder Defined by Eq. (3.136) [-] for sphere
$\boldsymbol{d_i}$	Recursive relation Defined by Eq. (3.66) [-] for cylinder Defined by Eq. (3.137) [-] for sphere
$\boldsymbol{e_i}$	Recursive relation, defined by Eq. (3.72) [-] for cylinder

LIST OF ABBREVIATIONS

$\boldsymbol{f_i}$	Recursive relation, defined by Eq. (3.73) [-] for cylinder
$\boldsymbol{p_i^o}$	$= c_i/c_n\,(p_n) + [e_i - (e_n/c_n)c_i]p_0$ $[Pa]$ for cylinder
$\boldsymbol{\omega_i}$	$= [f_i - (f_n/c_n)c_i]p_0$ $[Pa]$ for cylinder
$\boldsymbol{\chi_1}$	Axial strain term, defined by Eq. (3.78) $[m^2Pa]$ for cylinder
$\boldsymbol{\chi_2}$	Axial strain term, defined by Eq. (3.79) $[m^2Pa]$ for cylinder

CHAPTER 1

INTRODUCTION

1.1. Background of Study

Pressure vessel is a common equipment used in different industries for storing and transporting energy because more energy can be stored through compression of fluid (Mukherjee, 2019). It plays an important role in power production industry where higher operating pressure and temperature brings better thermal efficiency (Ohji and Haraguchi, 2017). Other than that, pressure vessel can be built for lethal services where it is used to contain corrosive or poisonous fluid (ASME, 2017). Owing to the hazardous operating nature of pressure vessel, prevention of pressure vessel's failure has been a major area of study since early days and it has been a growing concern (Lancaster, 1973).

One of the main strategies to run pressure vessel under harsh conditions is to construct cladded or coated pressure vessel, composite pressure vessel or functionally graded material (FGM) pressure vessel. These pressure vessels with multilayered design provides better resistance to high temperature, high pressure, corrosive and erosive environment with lower weight. Therefore, pressure vessel with multilayered design is often used in industries with extreme operating conditions such as cryogenic services, compressed gas services, aerospace industry, marine industry and power generation industry (El-Galy et

al., 2019; Mahamood and Akinlabi, 2017). In general, these pressure vessels are in cylindrical and spherical shapes. The spherical shape structure can evenly distribute the stresses due to its uniform profile. Therefore, the spherical shape structure can be made thinner as compared to cylindrical shape. Moreover, it has low surface area-to-volume ratio which is beneficial for storage application because it minimizes heat transfer to the surrounding as compared to other pressure vessel profiles. However, the fabrication of spherical pressure vessel is costly and difficult. Thus, cylindrical shape pressure vessel is the alternative option that provides combination of acceptable performance, economical and flexible construction (Megyesy and Buthod, 2008; Toudehdehghan and Hong, 2019).

1.2. Importance of Study

Multilayered pressure vessel is designed to work in harsh conditions where failure of the vessel during operation can cause great financial loss and put human lives at stake (Spence and Nash, 2004). So, it is important to evaluate the structural integrity of multilayered pressure vessel where an essential part of evaluating the structural integrity is to obtain the stresses induced within the wall of multilayered pressure vessel.

The analysis of multilayered pressure vessel's structure can be done through analytical and numerical method. However, when the number of layer of vessel's wall to be analyzed increases, obtaining the solution through analytical mean is more efficient. It is straight-forward and required minimal

computing effort as compared to using numerical tools (Chen and Ding, 2001). Furthermore, the analytical equations formed the fundamental mathematical model that describes a physical phenomenon. Based on the analytical equations, design codes and numerical tools are developed as the straightforward and practical alternatives to design and analyze a structure. Therefore, exploring analytical solution not only helps in understanding a physical phenomenon, it also provides more insight into the relevant design codes and numerical tools.

Due to the complex structure and running conditions of multilayered pressure vessel, the mathematical derivation involved in obtaining the stresses and displacements induced is complicated (Wang et al., 2012). There are researchers that explored different methodologies to realize the analysis of multilayered pressure vessel through analytical mean. From the literature survey, Shi et al. (2007) and Yeo et al. (2017) claimed that analytical solution derived based on recursive algorithm is simple, convenient and computationally efficient. Thus, proposing the analytical solution based on recursive algorithm to obtain the stresses induced within the wall of multilayered pressure vessel seems to be promising and feasible.

1.3. Problem Statement

Many researchers have explored the methodology to evaluate the performance of composite vessels and pipes under extreme environment based on analytical method. Recently, some researchers have introduced an efficient recursive algorithm to solve the thermo-mechanical problem of multilayered

hollow cylinder. The method was first reported by Shi et al. (2007) and later Yeo et al. (2017) modified the recursive algorithm to solve the thermo-mechanical problem of multilayered hollow cylinder. However, the solution proposed by Yeo et al. (2017) only applicable for plane strain condition where the axial strain has been ignored. Unlike tube and pipe, cylindrical pressure vessel comes with closed ends and the thermo-mechanical stress-strain of a multilayered pressure vessel will be affected by the axial strain developed due to the closed end design of the vessel (Wang et al., 2012). Besides that, no literature has reported the thermo-elastic formulation of multilayered spherical pressure vessel. Thus, the focus of the project is on the derivation of analytical solutions for determining the stresses distribution of multilayered cylindrical pressure vessel with closed ends and spherical pressure vessel that are subject to thermal and pressure loading.

1.4. Aim and Objectives

The aim of this research is to develop an analytical solution to solve the stresses of multilayered cylindrical and spherical pressure vessel under thermo-mechanical loading based on recursive algorithm. Listed below are the objectives to be achieved in this project:

1) To derive the analytical solution based on recursive algorithm for multilayered hollow cylindrical and spherical pressure vessels under steady state thermo-mechanical loading.
2) To compare results obtained by using the proposed analytical solutions with the finite element results.

3) To evaluate the proposed analytical solutions to approximate the solution for the thermo-mechanical problem of cylindrical and spherical pressure vessel made of functionally graded material (FGM).

1.5. Scope of Dissertation

This project focus on developing an analytical solution to identify stresses within the hollow cylindrical and spherical multilayered pressure vessel under steady state thermo-mechanical loadings. The assumptions, boundary conditions and interface conditions are first defined. Subsequently, a novel recursive algorithm is introduced to formulate the analytical solutions to solve the multilayered cylindrical and spherical pressure vessel problems. Next, the derived analytical solutions are validated through comparison with the results obtained from finite element analysis based on models reported in literatures. Lastly, the validated analytical solutions are demonstrated as an alternative solution to examine the stresses of FGM cylindrical and spherical pressure vessel reported in literatures.

1.6. Outline of Dissertation

Firstly, Chapter 1 shows the background of study, importance of study and problem statement followed by the aim and objectives of the current research. Based on these introductory content of the research, the relevant literatures are discussed and reviewed.

Next, Chapter 2 presents the literature survey on the background of pressure vessel, multilayered pressure vessel, analysis of pressure vessel's design and theories involved in deriving the analytical equations.

Chapter 3 describes the derivation of the proposed analytical solutions. It starts with defining the assumptions, notations, boundary conditions and interface conditions, followed by the derivation of analytical solution for temperature and stresses distribution for multilayered cylindrical pressure vessel. Finally, the derivation of analytical solution for temperature and stresses distribution for multilayered spherical pressure vessel are proposed.

Subsequently, the validation of the derived analytical solutions is carried out in Chapter 4. Two models adopted from literatures are constructed and the results generated by using the proposed analytical solutions and finite element analysis are compared and verified. The validated analytical solutions are used as the alternative solution to approximate the analytical solutions for FGM pressure vessels and the results are compared with the findings reported in literatures.

Finally, all findings are summarized in Chapter 5 along with the recommendation for future study.

CHAPTER 2

LITERATURE REVIEW

2.1. Pressure vessel

In general, any closed structure that contains pressure substantially different from ambient pressure is known as ‘pressure vessel’. It can come in different shapes such as cylindrical, spherical and conical. However, the common shapes of pressure vessel structure employed are sphere and cylinder. Spherical shape is favorable because it enables even stress distribution on both internal and external surface due to its uniform profile. It allows a thinner structure as compared to cylindrical shape. Other than that, spherical shape has a high volume-to-surface area ratio that minimizes heat transfer to surrounding. This is important when the pressure vessel is used to store fluid at temperature different from ambient. However, fabrication of spherical pressure vessel can be costly and difficult. Therefore, cylindrical pressure vessel became the more common option due to the ease of fabrication and flexibility (Toudehdehghan and Hong, 2019; Arslan et al., 2021). As compared to spherical shape, cylindrical shape gives better geometrical flexibility because both length and diameter can be altered to set the volume of the cylindrical pressure vessel. On top of that, cylindrical pressure vessel comes with different end design to form the enclosure. Designer can balance between performance and cost to decide using which type of end design. In ascending order of the ability to resist

pressure, the main types of design for cylindrical pressure vessel closed end are flat, torispherical, semi ellipsoidal and hemispherical (Lawate and Deshmukh, 2015; Thattil and Pany, 2017; ASME, 2017). Figure 2.1 and 2.2 illustrate a cylindrical and spherical pressure vessel.

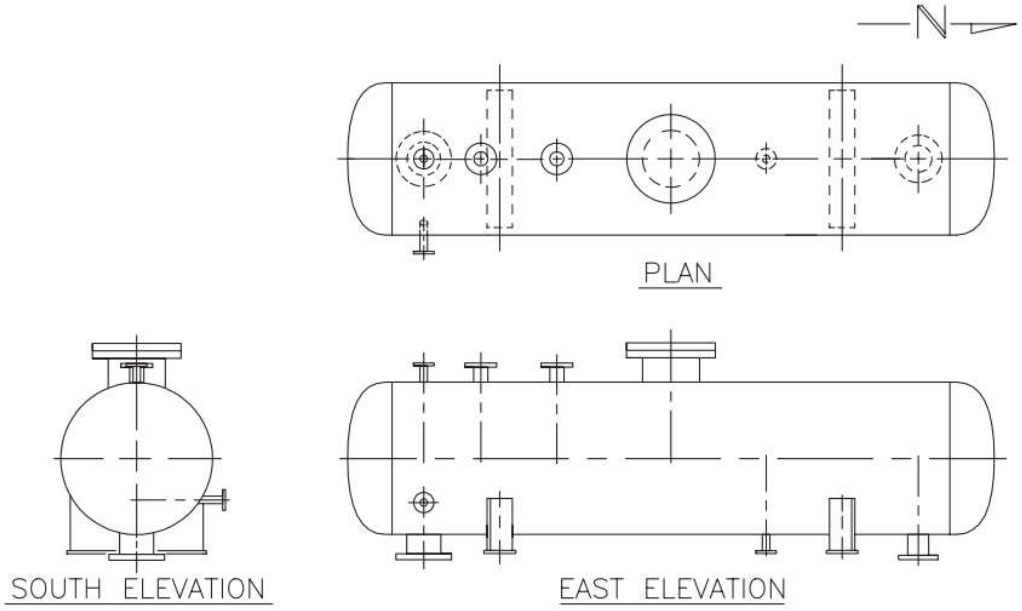

Figure 2.1: Plan and elevation view of a horizontal pressure vessel (Parisher and Rhea, 2012)

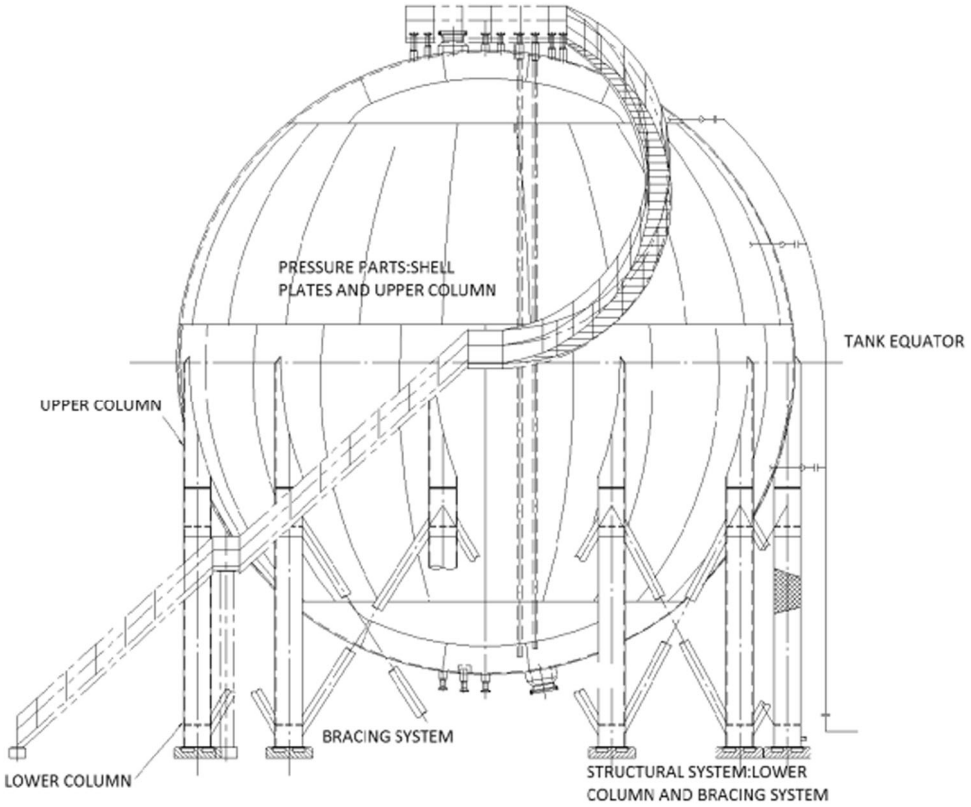

Figure 2.2: Elevation view of a spherical pressure vessel (Arabzadeh et al., 2018)

There is a wide range of material selection that can be used to construct pressure vessel, for example metal alloys, engineering composites, engineering polymers, ceramics and so on. Metal alloys such as carbon steels, low alloy steels and stainless steels are commonly used to construct pressure vessel because of the material's ductility and toughness that help in resisting sudden rupture (Chattopadhyay, 2008). The vessel's wall thickness will increase with higher operating temperature and pressure. When the operating environment gets more challenging, increasing wall thickness of single layer or solid wall vessel became impractical and is no longer economically feasible (Khurmi and Gupta, 2005).

2.2. Analysis of Pressure Vessel's Design

Pressurized equipment contained high density energy and hence any failure of it can be a catastrophic event. The incident shown in Figure 2.3 is the boiler explosion on SS Sultana, it is one of the most infamous accident where it has caused the loss of 1238 lives in year 1865. Other than that, there are a lot of documented incidents that have led to the initial development of design rule to govern and regulate the construction of pressure vessel (Spence and Nash, 2004). It is observable that the established design rule such as design codes, standards and acts has helped to reduce the number of failure cases since the passing of factory act in different countries during 1800s (Vakkilainen, 2017). These codes and standards are developed from theoretical knowledge, experimental results, numerical study and industry's practical experience. It is the compilation of existing knowledge that is used to ensure reliable construction of pressure vessel. It covers different aspects in the realization of pressure vessel construction. Taking ASME BPVC Section VIII for example, it provides prohibition and recommended practice for the design, fabrication and inspection of unfired pressure vessel (ASME, 2017). Still, there are parts that are not spelled out in pressure vessel design code due to the wide range of design parameters that can be manipulated such as uncommon shape, material, joint, operating conditions and so on. The verification of these new scenarios needs to be done through either analytical, numerical or experimental mean (ASME, 2017). For instance, Li et al. (2020) conducted the experiment to study the bursting of small-sized pressure vessel containing high pressure carbon dioxide for vessel explosion type named 'boiling liquid expanding vapor explosion'. By attaching small

spherical steel balls as prefabricated fragments on to the V-shaped grooves and X-shaped grooves of the pressure vessel, the bursting data can be collected through the dispersion and distribution of these prefabricated fragments. Other than that, Zhang et al. (2018b) studied the effect of cold-stretching on buckling behavior of cylindrical vessel under external pressure by using experimental and numerical simulation method. Sample vessels were fabricated by using different out-of-roundness ratio under both cold-stretching and without cold-stretching conditions. The vessels were scanned by using 3D laser scanner to convert into FEM model and the generated results from experiment and numerical simulation agreed with each other. On the other hand, Abdalla and Casagrande (2020) derived a novel analytical solution based on augmented Lagrangian formalism and Euler-Lagrange equation for the optimization problem of thickness distribution of axisymmetric pressure vessel.

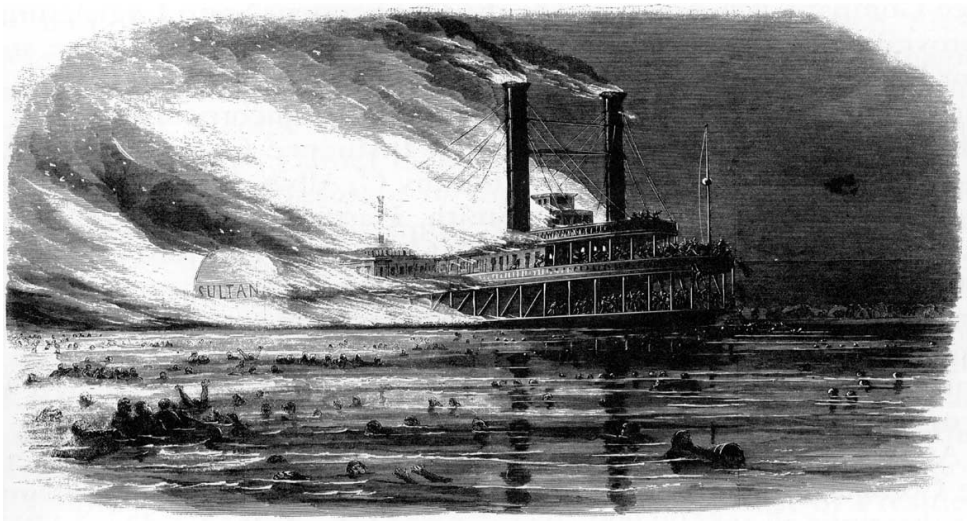

Figure 2.3: SS Sultana's boiler explosion (Spence and Nash, 2004)

Generally, the loadings on pressure vessel can be categorized into two types which are pressure loadings and applied forces (Bergman and Calif, 1955).

Among these loadings, pressure and thermal are the common and dominant loadings. ASME (2017) has been determining the wall thickness of pressure vessel based on limiting the structure's hoop stress to a certain proportion of material's yield strength, ultimate strength or creep rate. It is known as 'allowable stress' of the material at elevated temperature (Braun, 1969; ASME, 2017). On top of the steady state thermo-mechanical loading, users need to select the appropriate analytical procedures if there are other significant stresses induced due to special loadings such as wind or seismic loading, geometrical profile that will cause localized stresses and so on. In general cases, the effect of other minor factors are accounted by the safety factor in material strength and the set of design rules (Moss, 2004).

2.3. Multilayered Pressure Vessel and Other Multilayered Engineering Applications

Witolla et al. (2016) highlighted that one of the key features for the future of pressure vessel is the development of new material used in fabricating pressure vessel. Generally, factors that influence material selection of pressure vessel are material's strength, resistance to corrosion, fracture toughness, workability, availability and economical consideration (Toudehdehghan and Hong, 2019). With the advancement of fabrication technology, a good strategy to run pressure vessel under challenging environment is to construct multilayered pressure vessel such as coated or cladded, composite and functionally graded material (FGM) pressure vessel.

Solid wall vessel can be cladded or coated so that it can have different internal and/or external surfaces designed to resist pressure, temperature and chemical attack (Zhang et al., 2012; Wang et al., 2015). This case can be analyzed as a multilayered scenario. For example, Reinders et al. (2019) constructed a thermally insulated tank containing a compressed liquefied gas as a multilayered model and described the tank thermal model to predict pressure and temperature behavior of the tank when it is exposed to heat.

Composite pressure vessel offers better performance with lighter weight as compared to conventional metal alloys vessel (Rao et al., 2012; Nikbakht et al., 2018). This is because individual materials can be combined in a vast range of combinations to enable us to make better use of the materials' virtues while minimizing the materials' deficiencies (Harris, 1999). These materials are known as composite material and it is an extension to conventional material such as plastics, ceramics and metals. It is a multiphase material made from two or more constituents that gives unique properties (Mukherjee, 2019). This is also the reason that composite pressure vessel has better flexibility because it has wider range of parameters that can affect its structural behavior as compared to isotropic material. Composite pressure vessel can be viewed as a multilayered structure where the wall of the vessel is constructed by bonding different layers of laminates (Zhang et al., 2012; Mahdy et al., 2013; Wang et al., 2012). The application of composite pressure vessel are vessel that is used for gaseous hydrogen storage (Nebe et al., 2021) and vessel that is used to contain high pressure fluid in aerospace's propulsion system (Alam et al., 2020).

Next, FGM is an advanced type of composite material where the material properties were tailored to vary gradually with space. It helps to eliminate the sharp transition of material properties at interface of multilayered construction that can cause delamination due to discontinuity stress which is a common problem when using composite material for structural purpose (Bhavar et al., 2017; Toudehdehghan and Hong, 2019; Zhang et al., 2012). In addition, FGM pressure vessel can have different types of material properties variation function such as linear function, exponential function, power-law function and sigmoid function which can be optimized to suit to different operating scenarios (Nikbakht et al., 2019; Gupta and Talha, 2015). As per what reported by Mahamood and Akinlabi (2017) and El-Galy et al. (2019), some examples of application of FGM are in defense, armory, aerospace and automobile fields. Although FGM's technology is yet to be used in industrial scale, FGM has a promising future in application with harsh working environment such as pressure vessel, heat exchanger, heat component, rocket heat shield and so on.

Other than cylindrical pressure vessel, there are other multilayered hollow cylindrical structure that is common in engineering applications. For example, Figure 2.4 shows an underground gas well wall that is formed by layers of casing and cement. Zhang et al. (2017) studied the interaction between casing-cement sheath-surrounding rocks of underground gas well where it is taken as a multilayered cylindrical model. They analyzed the cement sheath integrity based on elastoplastic theory because failure of cement sheath due to varying pressure and temperature has been a major problem. Other than that, insulated pipe, coated pipe or composite pipe problems are often considered by

researchers as multilayered long cylinder scenario (Fraldi et al., 2016; Yeo et al., 2017).

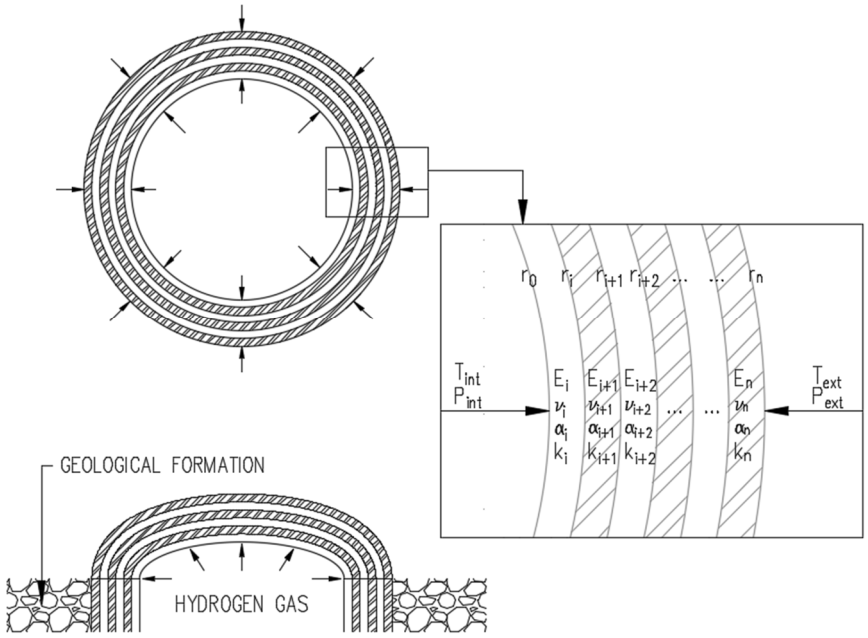

Figure 2.4: Illustration of underground gas well as multilayered hollow cylinder scenario

2.4. Analytical Works to Obtain Temperature Distribution and Stresses of Multilayered Pressure Vessel

The emergence of composite and FGM material has attracted the interest of researchers to investigate structures made of these materials. Among these literatures, researchers studied and presented different analytical methods used to analyze cylindrical and spherical composite and FGM pressure vessel under varies operating conditions. Ghajar and Cengel (2014) gave a good overall representation of mathematical modeling of physical problems in Figure 2.5. Researchers have been considering different variables, assumptions, solution

technique, initial and boundary conditions in their works.

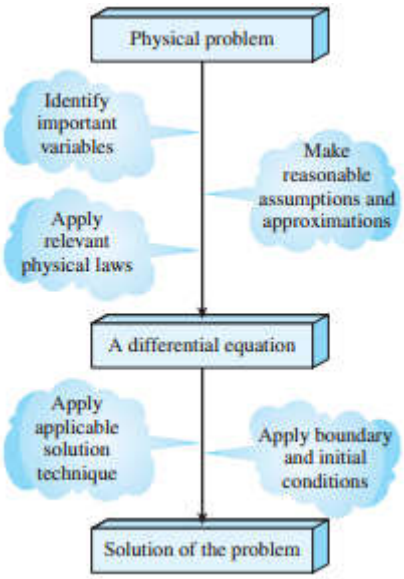

Figure 2.5: Mathematical modeling of physical problem (Ghajar and Cengel, 2014)

There is a vast amount of publications that have demonstrated the analysis of composite and FGM cylindrical pressure vessel through analytical mean. For example, Zimmerman and Lutz (1999) presented an exact solution for the problem of uniformly heated FGM cylinder where the elastic modulus and thermal expansion coefficient of the cylinder vary linearly with radius. Zhang et al. (2012) obtained the analytical solution of thermo-mechanical stresses in a multilayered composite cylindrical pressure vessel with the inclusion of closed-end effect. Nejad et al. (2016) has shown that for cylindrical pressure vessel fabricated by exponentially varying material, the governing differential equation is a second order homogenous differential equation that can be solved by using hypergeometric function. Recently, Benslimane et al. (2021) presented an analytical solution that can be used to obtain the mechanical

displacements and stresses in a thick-walled FGM cylindrical pressure vessel under axisymmetric mechanical loading within uniform magnetic field. A general expression of elastic modulus and magnetic permeability variation is used where it can be applicable to homogenous, power-law and exponentially varying material properties in radial direction. They derived and solved the second-order Navier's equation with the inclusion of Lorentz force resulted from the magnetic field to determine the displacements and stresses. Similarly, considerable amount of literatures was published that studied the structural performance of spherical composite and FGM pressure vessel. For example, Chen and Lin (2008) presented the analytical solution for cylindrical and spherical FGM under pressure loading where the material's elastic modulus was taken as an exponential function in radial direction. Also, Bayat et al. (2012) derived the analytical solution to solve thermo-mechanical problem of FGM hollow sphere where the material's elastic modulus, thermal expansion coefficient and thermal conductivity are expressed as power law functions in radial direction. Under the framework of small displacement and Von Mises yield criterion, Akış (2017) obtained the analytical solution to predict the yielding of two-layer composite spherical pressure vessel under either internal or external pressure. The recent work by Delouei et al. (2020) has given the analytical solution to solve two dimensional steady state heat transfer problem in a FGM hollow sphere. The conductivity coefficient was treated to be different in both radial and peripheral directions. Along with general internal and external thermal boundary conditions, the derived solutions were in the form of Bessel and Legendre functions.

Researchers have been working on multilayered structure since 1950-an (Habip, 1965). Out of all the analytical solutions published to solve multilayered problem, Shi et al. (2007), Vedeld and Sollund (2014) and Yeo et al. (2017) reported that recursive algorithm is simple and efficient to be applied in solving multilayered structure problem. Shi et al. (2007) proposed a simple recursive algorithm to solve for the radial and tangential stresses distribution across multilayered hollow cylindrical wall loaded with uniform inner and outer pressure. On top of the work by Shi et al. (2007), Vedeld and Sollund (2014) considered axial loading and thermal stresses across a multilayered hollow cylinder, but the temperature distribution was assumed to be uniform across the multilayered hollow cylinder. Yeo et al. (2017) extended the analytical solutions reported by Shi et al. (2007) and Vedeld and Sollund (2014). They proposed an analytical solution for multilayered hollow cylinder under thermo-mechanical loading where heat conduction across the cylindrical wall has been considered with radial temperature variation. Yet, the analytical solution proposed by Yeo et al. (2017) was under plane strain assumption which is suitable to describe the cross section of a long cylinder far from any closed end where the axial strain is insignificant. For cylindrical pressure vessel, the axial strain is significant due to the mechanical loading on the closed end and the thermal loading on the overall structure (Wang et al., 2012). Also, the analytical solution to solve thermo-mechanical problem of multilayered spherical pressure vessel has not been presented in any literature.

2.5. Heat Conduction Equations in Cylindrical and Spherical Coordinate

Energy can exist in different forms. When there is spatial temperature difference, there is a driving force to transfer energy from higher temperature system to lower temperature system. This form of energy transfer is termed as 'heat' and an example phenomenon is the cooling of a cup of hot tea to ambient temperature. Heat energy originated from the internal energy of molecules where the part associated with the kinetic energy of molecules is known as sensible heat and the intermolecular forces between molecules that determine the phase of the system is known as latent heat. Like what shown in Figure 2.6, there are three ways of heat transfer which are conduction, convection and radiation (Bergman et al., 2011; Ghajar and Cengel, 2014).

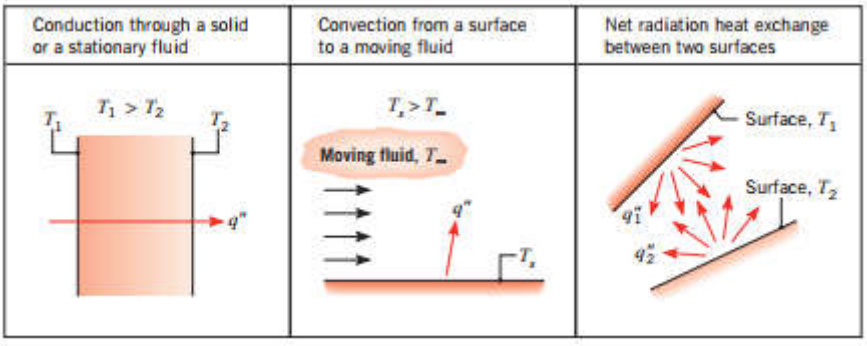

Figure 2.6: Conduction, convection and radiation heat transfer (Bergman et al., 2011)

Conduction is the transfer of energy from high energy particles to low energy particles through interactions between the particles. In solid, conduction occurs due to the combined effect of molecules' lattice vibration and energy

transport by free electrons. Fourier's law of heat conduction is the fundamental experimental law of heat transfer which was published by Joseph Fourier in year 1822. It stated that the one directional rate of heat transfer per unit area through a plane layer is proportional to the temperature difference across the layer, yet inversely proportional to the layer's thickness. Mathematically, it is expressed as Eq. (2.1) where $q^{"}$ is the conduction heat flux rate, k is the layer's thermal conductivity, $\frac{dT}{dx}$ is the temperature gradient across the layer and the negative sign indicates that the heat flow is in the opposing direction of the temperature gradient (Bergman et al., 2011; Ghajar and Cengel, 2014).

$$q^{"} = -k\frac{dT}{dx} \tag{2.1}$$

On top of the Fourier's law of heat conduction, the general heat conduction governing equation needs to be derived based on the principle of conservation of energy applied to a differential control volume in order to identify the temperature field for a solid subjected to thermal loading (Bergman et al., 2011).

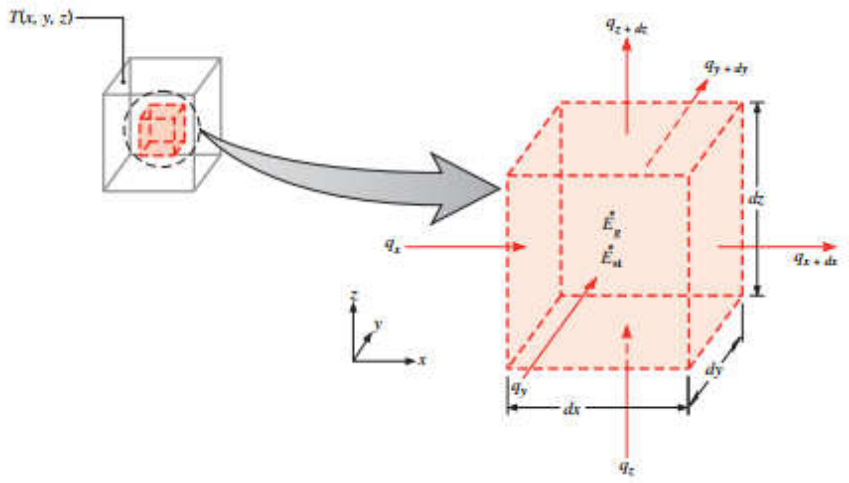

Figure 2.7: Rectangular differential control volume for heat conduction analysis (Bergman et al., 2011)

Figure 2.7 shows a three dimensional rectangular differential control volumes where there are energy conduction terms E_{in} and E_{out}, energy generation term E_g and energy storage term E_{st}. Applying the principle of conservation of energy

$$E_{in} + E_g - E_{out} = E_{st} \tag{2.2}$$

for

$$q_x = q_x'' dydz = -kdydz\frac{\partial T}{\partial x} \tag{2.3}$$

$$q_y = q_y'' dxdz = -kdxdz\frac{\partial T}{\partial y} \tag{2.4}$$

$$q_z = q_z'' dxdy = -kdxdy\frac{\partial T}{\partial z} \tag{2.5}$$

Thus, the governing equation in Cartesian coordinate can be written as

$$\frac{\partial}{\partial x}\left(k\frac{\partial T}{\partial x}\right)+\frac{\partial}{\partial y}\left(k\frac{\partial T}{\partial y}\right)+\frac{\partial}{\partial z}\left(k\frac{\partial T}{\partial z}\right)+R=\rho c\frac{\partial T}{\partial t} \tag{2.6}$$

where x, y, z, T, k, R, ρ, c and t are length of control volume, width of the control volume, height of the control volume, temperature, thermal conductivity, energy generated per unit volume, density, specific heat capacity and time respectively (Bergman et al., 2011).

Figure 2.8 shows the convention of rectangular, cylindrical and spherical coordinate. Since this research work studied about cylindrical and spherical pressure vessel, it is convenient to express the governing equation in terms of cylindrical and spherical coordinate. By using similar approach, the principle of conservation of energy is applied to differential volume taken in terms of cylindrical and spherical coordinate, Eq. (2.7) is the heat conduction governing equation written in cylindrical coordinate while Eq. (2.8) is in spherical coordinate (Bergman et al., 2011).

$$\frac{1}{r}\frac{\partial}{\partial \mathrm{r}}\left(kr\frac{\partial T}{\partial r}\right)+\frac{1}{r^2}\frac{\partial}{\partial \emptyset}\left(k\frac{\partial T}{\partial \emptyset}\right)+\frac{\partial}{\partial \mathrm{z}}\left(k\frac{\partial T}{\partial z}\right)+R=\rho c\frac{\partial T(t)}{\partial t} \tag{2.7}$$

$$\frac{1}{r^2}\frac{\partial}{\partial r}\left(kr^2\frac{\partial T}{\partial r}\right)+\frac{1}{r^2\sin^2\theta}\frac{\partial}{\partial \emptyset}\left(k\frac{\partial T}{\partial \emptyset}\right)+\frac{1}{r^2\sin\theta}\frac{\partial}{\partial \theta}\left(k\sin\theta\frac{\partial T}{\partial \theta}\right)+R=\rho c\frac{\partial T(t)}{\partial t} \tag{2.8}$$

where r, $\emptyset$ and θ are radius, azimuthal angle and polar angle.

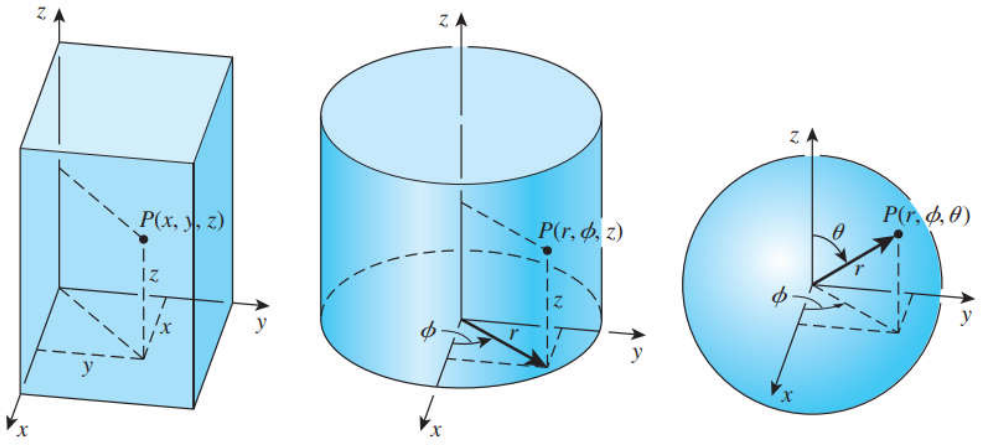

Figure 2.8: Rectangular, cylindrical and spherical coordinates (Ghajar and Cengel, 2014)

2.6. Thermoelasticity

The primary function of engineering structure is to support or transfer external load. Stresses developed when the structure is loaded. For a force ΔF acting on surface ΔA, the stress, σ can be defined as what shown in Eq. (2.9) and it can be resolved into normal and shear components (Boresi and Schmidt, 2009).

$$\sigma = \lim_{\Delta A \to 0} \frac{\Delta F}{\Delta A} \tag{2.9}$$

In order to identify the load-stress relations, three conditions need to be derived that are the equations of equilibrium, the compatibility or continuity conditions and the constitutive relations. For a loaded structure that has zero acceleration, the differential equations of motion of a deformable body described the equilibrium state of the body. Other than that, the geometrical

compatibility or continuity conditions need to be complied and these are represented by strain compatibility equations and strain-displacement relations. Lastly, the constitutive equation gives the material response when it is loaded. It is the material's stress-strain relations and thus the load-stress relations can be identified (Boresi and Schmidt, 2009).

As shown in Figure 2.9 is a rectangular deformable body where the differential equations of motion of the deformable body can be obtained through summation of forces and moments.

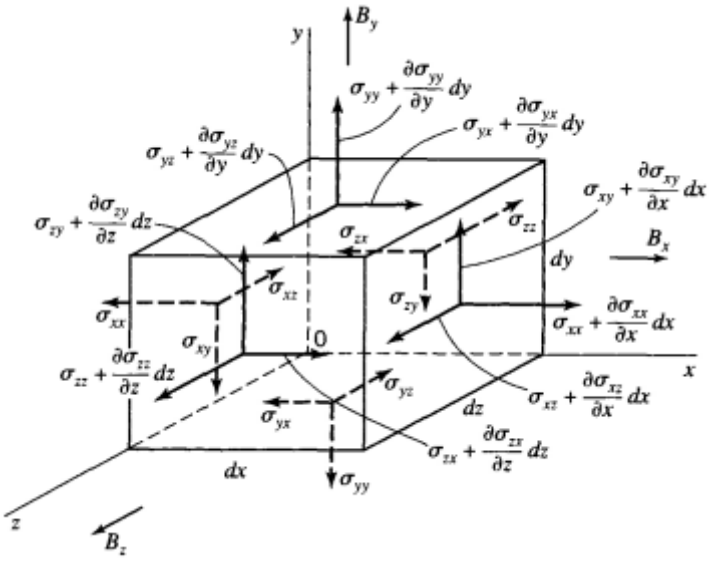

Figure 2.9: Stresses components with body force in rectangular coordinate (Boresi and Schmidt, 2009)

For B_x, B_y and B_z being the body forces per unit volume in the respective directions, σ_{xx}, σ_{yy} and σ_{zz} being normal stresses in the respective directions, σ_{xy}, σ_{yx}, σ_{xz}, σ_{zx}, σ_{yz} and σ_{zy} being shear stresses in the respective directions, the different equations of motion are

$$\frac{\partial \sigma_{xx}}{\partial x} + \frac{\partial \sigma_{yx}}{\partial y} + \frac{\partial \sigma_{zx}}{\partial z} + B_x = 0 \tag{2.10}$$

$$\frac{\partial \sigma_{xy}}{\partial x} + \frac{\partial \sigma_{yy}}{\partial y} + \frac{\partial \sigma_{zy}}{\partial z} + B_y = 0 \tag{2.11}$$

$$\frac{\partial \sigma_{xz}}{\partial x} + \frac{\partial \sigma_{yz}}{\partial y} + \frac{\partial \sigma_{zz}}{\partial z} + B_z = 0 \tag{2.12}$$

Stresses aroused due to deformation of a deformable body, the deformation needs to be identified to apply the theory of elasticity. Under small-displacement theory, the strain-displacement relations are (Boresi and Schmidt, 2009)

$$\epsilon_{xx} \approx \frac{\partial u_x}{\partial x} \tag{2.13}$$

$$\epsilon_{yy} \approx \frac{\partial u_y}{\partial y} \tag{2.14}$$

$$\epsilon_{zz} \approx \frac{\partial u_z}{\partial z} \tag{2.15}$$

$$\epsilon_{xy} \approx \frac{1}{2}\left(\frac{\partial u_y}{\partial x} + \frac{\partial u_x}{\partial y}\right) \tag{2.16}$$

$$\epsilon_{xz} \approx \frac{1}{2}\left(\frac{\partial u_z}{\partial x} + \frac{\partial u_x}{\partial z}\right) \tag{2.17}$$

$$\epsilon_{yz} \approx \frac{1}{2}\left(\frac{\partial u_z}{\partial y} + \frac{\partial u_y}{\partial z}\right) \tag{2.18}$$

where ϵ_{xx}, ϵ_{yy} and ϵ_{zz} are normal strains in respective directions, ϵ_{xy}, ϵ_{xz} and ϵ_{yz} are shear strains in respective directions, u_x, u_y and u_z are displacements in respective directions. As shown below, the strain compatibility equations of

small-displacement theory can be obtained by elimination of the displacement components (Boresi and Schmidt, 2009).

$$\frac{\partial^2 \epsilon_{yy}}{\partial x^2} + \frac{\partial^2 \epsilon_{xx}}{\partial y^2} = 2\frac{\partial^2 \epsilon_{xy}}{\partial x \partial y} \tag{2.19}$$

$$\frac{\partial^2 \epsilon_{zz}}{\partial x^2} + \frac{\partial^2 \epsilon_{xx}}{\partial z^2} = 2\frac{\partial^2 \epsilon_{xz}}{\partial x \partial z} \tag{2.20}$$

$$\frac{\partial^2 \epsilon_{zz}}{\partial y^2} + \frac{\partial^2 \epsilon_{yy}}{\partial z^2} = 2\frac{\partial^2 \epsilon_{yz}}{\partial y \partial z} \tag{2.21}$$

$$\frac{\partial^2 \epsilon_{zz}}{\partial x \partial y} + \frac{\partial^2 \epsilon_{xy}}{\partial z^2} = \frac{\partial^2 \epsilon_{yz}}{\partial z \partial x} + \frac{\partial^2 \epsilon_{zx}}{\partial y \partial z} \tag{2.22}$$

$$\frac{\partial^2 \epsilon_{yy}}{\partial x \partial z} + \frac{\partial^2 \epsilon_{xz}}{\partial y^2} = \frac{\partial^2 \epsilon_{yz}}{\partial z \partial x} + \frac{\partial^2 \epsilon_{zx}}{\partial y \partial z} \tag{2.23}$$

$$\frac{\partial^2 \epsilon_{xx}}{\partial y \partial z} + \frac{\partial^2 \epsilon_{yz}}{\partial x^2} = \frac{\partial^2 \epsilon_{xz}}{\partial x \partial y} + \frac{\partial^2 \epsilon_{xy}}{\partial x \partial z} \tag{2.24}$$

Subsequently, the stress-strain relations need to be obtained. By using principle of conservation of energy, the work done by the stress can be related to the change in internal energy that is expressed in terms of strains. For small displacement linear elastic isotropic material, the stresses can be written in terms of the sum of principal strains which is an invariant and the strains in the same direction as the stresses. Therefore, the expression of Eq. (2.26) to Eq. (2.37) is generally applicable for any orthogonal curvilinear spatial coordinates (Boresi and Schmidt, 2009).

When an isotropic elastic continuum is exposed to thermal loading, it has a field of temperature distribution. When the unconstrained isotropic elastic

continuum is experiencing a uniform small increase in temperature, it is observed that all line elements in the volume undergo equal expansions and the line elements maintain their initial directions (Boresi and Schmidt, 2009; Hetnarski and Eslami, 2009).

$$\epsilon_T = \alpha\Delta \tag{2.25}$$

where α is the thermal expansion coefficient and Δ is the temperature difference measured against the material reference temperature.

The thermal effect is included in the stress-strain relations where

$$\epsilon_{xx} = \frac{1}{E}\left(\sigma_{xx} - \nu\sigma_{yy} - \nu\sigma_{zz}\right) + \alpha\Delta \tag{2.26}$$

$$\epsilon_{yy} = \frac{1}{E}\left(\sigma_{yy} - \nu\sigma_{xx} - \nu\sigma_{zz}\right) + \alpha\Delta \tag{2.27}$$

$$\epsilon_{zz} = \frac{1}{E}\left(\sigma_{zz} - \nu\sigma_{xx} - \nu\sigma_{yy}\right) + \alpha\Delta \tag{2.28}$$

$$\epsilon_{xy} = \frac{1+\nu}{E}\sigma_{xy} \tag{2.29}$$

$$\epsilon_{xz} = \frac{1+\nu}{E}\sigma_{xz} \tag{2.30}$$

$$\epsilon_{yz} = \frac{1+\nu}{E}\sigma_{yz} \tag{2.31}$$

and

$$\sigma_{xx} = \frac{E}{(1+\nu)(1-2\nu)}\left[(1-\nu)\epsilon_{xx} + \nu\left(\epsilon_{yy} + \epsilon_{zz}\right) - (1 + \nu)\alpha\Delta\right] \tag{2.32}$$

$$\sigma_{yy} = \frac{E}{(1+\nu)(1-2\nu)}\left[(1-\nu)\epsilon_{yy} + \nu(\epsilon_{xx} + \epsilon_{zz}) - (1 + \nu)\alpha\Delta\right] \tag{2.33}$$

$$\sigma_{zz} = \frac{E}{(1+\nu)(1-2\nu)}\left[(1-\nu)\epsilon_{zz} + \nu\left(\epsilon_{xx} + \epsilon_{yy}\right) - (1 + \nu)\alpha\Delta\right] \tag{2.34}$$

$$\sigma_{xy} = \frac{E}{1+\nu}\epsilon_{xy} \tag{2.35}$$

$$\sigma_{xz} = \frac{E}{1+\nu}\epsilon_{xz} \tag{2.36}$$

$$\sigma_{yz} = \frac{E}{1+\nu}\epsilon_{yz} \tag{2.37}$$

where E and ν are elastic modulus and Poisson's ratio. The material properties are determined experimentally.

Relative to rectangular coordinate, Boresi and Schmidt (2009) gave the general differential equations of equilibrium and strain-displacement relations of small displacement theory in any orthogonal curvilinear spatial coordinates where α_c, β_c and γ_c are metric coefficients that are different for different coordinate systems.

$$\frac{\partial(\beta_c\gamma_c\sigma_{xx})}{\partial x}+\frac{\partial\left(\gamma_c\alpha_c\sigma_{yx}\right)}{\partial y}+\frac{\partial(\alpha_c\beta_c\sigma_{zx})}{\partial z}+\gamma_c\sigma_{yx}\frac{\partial\alpha_c}{\partial y} \tag{2.38}$$

$$+\beta_c\sigma_{zx}\frac{\partial\alpha_c}{\partial z}-\gamma_c\sigma_{yy}\frac{\partial\beta_c}{\partial x}-\beta_c\sigma_{zz}\frac{\partial\gamma_c}{\partial x}$$

$$+\alpha_c\beta_c\gamma_cB_x=0$$

$$\frac{\partial\left(\beta_c\gamma_c\sigma_{xy}\right)}{\partial x}+\frac{\partial\left(\gamma_c\alpha_c\sigma_{yy}\right)}{\partial y}+\frac{\partial\left(\alpha_c\beta_c\sigma_{zy}\right)}{\partial z}+\alpha_c\sigma_{zy}\frac{\partial\beta_c}{\partial z} \tag{2.39}$$

$$+\gamma_c\sigma_{xy}\frac{\partial\beta_c}{\partial x}-\alpha_c\sigma_{zz}\frac{\partial\gamma_c}{\partial y}-\gamma_c\sigma_{xx}\frac{\partial\alpha_c}{\partial y}$$

$$+\alpha_c\beta_c\gamma_cB_y=0$$

$$\frac{\partial(\beta_c\gamma_c\sigma_{xz})}{\partial x}+\frac{\partial\left(\gamma_c\alpha_c\sigma_{yz}\right)}{\partial y}+\frac{\partial(\alpha_c\beta_c\sigma_{zz})}{\partial z}+\beta_c\sigma_{xz}\frac{\partial\gamma_c}{\partial x} \tag{2.40}$$

$$+\alpha_c\sigma_{yz}\frac{\partial\gamma_c}{\partial y}-\beta_c\sigma_{xx}\frac{\partial\alpha_c}{\partial z}-\alpha_c\sigma_{yy}\frac{\partial\beta_c}{\partial z}$$

$$+\alpha_c\beta_c\gamma_cB_z=0$$

and

$$\epsilon_{xx}=\frac{1}{\alpha_c}\left(\frac{\partial u_x}{\partial x}+\frac{u_y}{\beta_c}\frac{\partial\alpha_c}{\partial y}+\frac{u_z}{\gamma_c}\frac{\partial\alpha_c}{\partial z}\right) \tag{2.41}$$

$$\epsilon_{yy}=\frac{1}{\beta_c}\left(\frac{\partial u_y}{\partial y}+\frac{u_z}{\gamma_c}\frac{\partial\beta_c}{\partial z}+\frac{u_x}{\alpha_c}\frac{\partial\beta_c}{\partial x}\right) \tag{2.42}$$

$$\epsilon_{zz}=\frac{1}{\gamma_c}\left(\frac{\partial u_z}{\partial z}+\frac{u_x}{\alpha_c}\frac{\partial\gamma_c}{\partial x}+\frac{u_y}{\beta_c}\frac{\partial\gamma_c}{\partial y}\right) \tag{2.43}$$

$$\epsilon_{xy}=\frac{1}{2}\left(\frac{1}{\beta_c}\frac{\partial u_x}{\partial y}+\frac{1}{\alpha_c}\frac{\partial u_y}{\partial x}-\frac{u_y}{\alpha_c\beta_c}\frac{\partial\beta_c}{\partial x}-\frac{u_x}{\alpha_c\beta_c}\frac{\partial\alpha_c}{\partial y}\right) \tag{2.44}$$

$$\epsilon_{xz}=\frac{1}{2}\left(\frac{1}{\alpha_c}\frac{\partial u_z}{\partial x}+\frac{1}{\gamma_c}\frac{\partial u_x}{\partial z}-\frac{u_x}{\alpha_c\gamma_c}\frac{\partial\alpha_c}{\partial z}-\frac{u_z}{\alpha_c\gamma_c}\frac{\partial\gamma_c}{\partial x}\right) \tag{2.45}$$

$$\epsilon_{yz}=\frac{1}{2}\left(\frac{1}{\beta_c}\frac{\partial u_z}{\partial y}+\frac{1}{\gamma_c}\frac{\partial u_y}{\partial z}-\frac{u_z}{\beta_c\gamma_c}\frac{\partial\gamma_c}{\partial y}-\frac{u_y}{\beta_c\gamma_c}\frac{\partial\beta_c}{\partial z}\right) \tag{2.46}$$

2.6.1. Thermoelasticity in Cylindrical Coordinate

Figure 3.2 illustrates the section view of a cylindrical pressure vessel. As referring to Eq. (2.38) to Eq. (2.46), $x = r$, $y = \emptyset$, $z = z$, $\alpha_c = 1$, $\beta_c = r$ and $\gamma_c = 1$ for cylindrical coordinate. Thus, the equations in cylindrical coordinate are (Boresi and Schmidt, 2009)

$$\frac{\partial \sigma_{rr}}{\partial r} + \frac{1}{r}\frac{\partial \sigma_{\emptyset r}}{\partial \emptyset} + \frac{\partial \sigma_{zr}}{\partial z} + \frac{\sigma_{rr} - \sigma_{\emptyset\emptyset}}{r} + B_r = 0 \tag{2.47}$$

$$\frac{\partial \sigma_{r\emptyset}}{\partial r} + \frac{1}{r}\frac{\partial \sigma_{\emptyset\emptyset}}{\partial \emptyset} + \frac{\partial \sigma_{z\emptyset}}{\partial z} + \frac{2\sigma_{r\emptyset}}{r} + B_\emptyset = 0 \tag{2.48}$$

$$\frac{\partial \sigma_{rz}}{\partial r} + \frac{1}{r}\frac{\partial \sigma_{\emptyset z}}{\partial \emptyset} + \frac{\partial \sigma_{zz}}{\partial z} + \frac{\sigma_{rz}}{r} + B_z = 0 \tag{2.49}$$

and

$$\epsilon_{rr} = \frac{\partial u_r}{\partial r} \tag{2.50}$$

$$\epsilon_{\emptyset\emptyset} = \frac{u_r}{r} + \frac{1}{r}\frac{\partial u_\emptyset}{\partial \emptyset} \tag{2.51}$$

$$\epsilon_{zz} = \frac{\partial u_z}{\partial z} \tag{2.52}$$

$$\epsilon_{r\emptyset} = \frac{1}{2}\left[\frac{1}{r}\frac{\partial u_r}{\partial \emptyset} + \frac{\partial u_\emptyset}{\partial r} - \frac{u_\emptyset}{r}\right] \tag{2.53}$$

$$\epsilon_{rz} = \frac{1}{2}\left(\frac{\partial u_r}{\partial z} + \frac{\partial u_z}{\partial r}\right) \tag{2.54}$$

$$\epsilon_{\emptyset z} = \frac{1}{2}\left(\frac{\partial u_\emptyset}{\partial z} + \frac{1}{r}\frac{\partial u_z}{\partial \emptyset}\right) \tag{2.55}$$

In a large class of engineering problems, the system can sometimes be simplified to plane stress, plane strain and generalized plane strain. However, these simplifications should be carried out with thorough consideration and evaluation to prevent inaccuracy in analysis since there is not a generally accepted criterion to determine what should be considered as plane stress, plane strain and generalized plane strain scenario (Mijuca, 2006; Kotousov and Wang, 2002).

2.6.2. Plane Stress, Plane Strain and Generalized Plane Strain Assumptions

'Plane stress' means that a loaded structure has negligible stress across a particular plane. Ideally, it should be applied to plate with vanishing thickness (Kotousov and Wang, 2002; Boresi and Schmidt, 2009). In actual case, it is commonly applied to very thin member where the generated axial stress is insignificant (Babuška and Szabó, 2006). For cylinder stress analysis, the definition of plane stress scenario is such that $\sigma_{zz} = \sigma_{rz} = \sigma_{\theta z} = 0$.

When a loaded structure has great length-to-section area ratio and shearing traction is negligible, it can be approximated as a case of plane strain (Wu and Li, 1990; Babuška and Szabó, 2006). In the context of analysis of cylinder, the condition for plane strain is such that $\epsilon_{zz} = \epsilon_{rz} = \epsilon_{\theta z} = 0$.

There are different definitions of generalized plane strain (Babuška and Szabó, 2006; Cheng et al., 1995). For this research work, the axial strain is taken

to be constant (Rencis and Huang, 1992; Zhang et al., 2012). All cross section of the multilayered cylindrical wall is expected to experience uniform axial displacement where ϵ_{zz} =constant. For pressure vessel, ϵ_{zz} can be obtained through summation of forces due the internal pressure, external pressure and axial stress induced within material. Also, thermal strain due temperature increment need to be included.

2.6.3. Thermoelasticity in Spherical Coordinate

Figure 3.3 depicts the section view of a spherical pressure vessel. The coordinate system and metric coefficients in Eq. (2.38) to Eq. (2.46) are such that $x = r$, $y = \theta$, $z = \emptyset$, $\alpha_c = 1$, $\beta_c = r$ and $\gamma_c = r\sin\theta$ for spherical coordinate. Thus, the equations in spherical coordinate are (Boresi and Schmidt, 2009)

$$\frac{\partial \sigma_{rr,i}}{\partial r} + \frac{1}{r}\frac{\partial \sigma_{\theta r,i}}{\partial \theta} + \frac{1}{r\sin\theta}\frac{\partial \sigma_{\emptyset r,i}}{\partial \emptyset} + \frac{1}{r}\left(2\sigma_{rr,i} - \sigma_{\theta\theta,i} - \sigma_{\emptyset\emptyset,i} + \sigma_{\theta r,i}\cot\theta\right) + B_r = 0 \tag{2.56}$$

$$\frac{\partial \sigma_{r\theta,i}}{\partial r} + \frac{1}{r}\frac{\partial \sigma_{\theta\theta,i}}{\partial \theta} + \frac{1}{r\sin\theta}\frac{\partial \sigma_{\emptyset\theta,i}}{\partial \emptyset} + \frac{1}{r}\left[\left(\sigma_{\theta\theta,i} - \sigma_{\emptyset\emptyset,i}\right)\cot\theta + 3\sigma_{r\theta,i}\right] + B_\theta = 0 \tag{2.57}$$

$$\frac{\partial \sigma_{r\emptyset,i}}{\partial r} + \frac{1}{r}\frac{\partial \sigma_{\theta\emptyset,i}}{\partial \theta} + \frac{1}{r\sin\theta}\frac{\partial \sigma_{\emptyset\emptyset,i}}{\partial \emptyset} + \frac{1}{r}\left(3\sigma_{r\emptyset,i} + 2\sigma_{\theta\emptyset,i}\cot\theta\right) + B_{\emptyset} = 0 \tag{2.58}$$

and

$$\epsilon_{rr} = \frac{\partial u_r}{\partial r} \tag{2.59}$$

$$\epsilon_{\theta\theta} = \frac{u_r}{r} + \frac{1}{r}\frac{\partial u_\theta}{\partial \theta} \tag{2.60}$$

$$\epsilon_{\emptyset\emptyset} = \frac{u_r}{r} + \frac{u_\theta}{r}\cot\theta + \frac{1}{r\sin\theta}\frac{\partial u_\emptyset}{\partial \emptyset} \tag{2.61}$$

$$\epsilon_{r\theta} = \frac{1}{2}\left[\frac{1}{r}\frac{\partial u_r}{\partial \theta} + \frac{\partial u_\theta}{\partial r} - \frac{u_\theta}{r}\right] \tag{2.62}$$

$$\epsilon_{r\emptyset} = \frac{1}{2}\left(\frac{1}{r\sin\theta}\frac{\partial u_r}{\partial \emptyset} + \frac{\partial u_\emptyset}{\partial r} - \frac{u_\emptyset}{r}\right) \tag{2.63}$$

$$\epsilon_{\theta\emptyset} = \frac{1}{2}\left[\frac{1}{r}\left(\frac{\partial u_\emptyset}{\partial \theta} - u_\emptyset\cot\theta\right) + \frac{1}{r\sin\theta}\frac{\partial u_\theta}{\partial \emptyset}\right] \tag{2.64}$$

2.7. Recursive Algorithm

Recursive algorithm is related to an importance mathematical concept called ‘induction’. It is used to obtain a parameter through function that has the parameter itself in its domain (Ferreira and Martins, 2009). It is also a common method used in computer-based application due to the computer strength in performing looping and counting function (Insa and Silva, 2015; Blass, 2016). Therefore, it has been applied regularly in solving engineering problems. Apart from the application of recursive algorithm demonstrated by Shi et al. (2007),

Vedeld and Sollund (2014) and Yeo et al. (2017), Zhang et al. (2018a) formulated a semi-analytical solution to obtain the three dimensional temperature field for multilayer system under unit point heat flux. The equations are derived by using thermal conduction equation in terms of frequency domain where the formed matrix of equations are solved recursively. Other than that, Naik et al. (2018) developed a novel finite difference based thermodynamic model for analyzing the variations of air and desiccant properties along the rates of water evaporation and condensation in dehumidifier and regenerator. The developed model is solved by using a proposed recursive algorithm.

2.8. Finite Element Method

The term 'Finite Element Method' (FEM) was used since year 1960. The popularity of using FEM for engineering analysis has increased ever since due to advancement of computer technology and its application. It is a numerical technique developed to solve differential equation or problem that can be formulated as functional minimized. By having finite set of equations, boundary and initial conditions, a system is described and defined (Knowles, 1984). The formulation of the finite element equations is based on variational principle where the difference between the approximated solution and the real solution is kept to minimal. For problem involves differential equation, the common method used is Galerkin method where the finite element equations formulation is based on residual minimization. It is crucial for user to understand the problem to be analyzed and FEM as a computational tool in order to perform an appropriate analysis. There are different types of element that can be grouped

into three general categories: line element (1D), planar element (2D) and solid element (3D). The validation of the proposed analytical solution in this work was done by using ANSYS FEM package. In the simulation performed, PLANE77 is a 2-D 8-Node thermal solid element that was used for the steady state thermal analysis. After that, the elements are converted to PLANE183. It is a 2-D 8-Node structural solid element that was used for the following thermal stress analysis (ANSYS, 2009). After creating a geometrical model, the general steps to use FEM are as below (Perumal and Mon, 2011):

1. Discretization of the model
2. Determining shape functions
3. Deriving the element equations
4. Assembling element equations to form the global equation
5. Solving the global equation
6. Results interpretation

FEM has been a popular method used in validating analytical solutions for engineering problems. Maleki et al. (2010) developed a theoretical model constructed using Variable Material Properties method for the case of residual stress analysis of autofrettaged spherical pressure vessel. They compared their results with FEM analysis results to evaluate the proposed theoretical model. Similarly, the exact solution of elastic analysis for functionally graded material cylindrical pressure vessel has been developed by Nejad et al. (2016). The exact solution can be used to identify radial and tangential stresses for cylindrical pressure vessel with exponentially varying material properties under plane strain condition. The developed exact solution was validated through comparison with FEM results.

2.9. Summary

The common shapes of pressure vessel are cylindrical and spherical (Toudehdehghan and Hong, 2019) and the common material used to construct pressure vessel are metal alloys (Chattopadhyay, 2008). The thickness of vessel's wall increases with higher operating temperature and pressure. Therefore, when the pressure vessel needs to work under extreme temperature and pressure for better thermal efficiency (Ohji and Haraguchi, 2017), fabricating single layer metal alloy pressure vessel is no longer practical and not economically feasible (Khurmi and Gupta, 2005). As the fabrication technology advances, the opportunity to deal with this challenge lies in constructing pressure vessel made of new material including pressure vessel with multilayered design such as coated or cladded, composite and FGM pressure vessel (Witolla et al., 2016).

Failure of pressure vessel can be a catastrophic event because it contains high density energy (Spence and Nash, 2004). Thus, assessing structural integrity of pressure vessel has been a subject of study since early days (Lancaster, 1973). Industry players have been designing and analyzing pressure vessel based on codes and standards. These codes and standards are the compilation of mankind's existing knowledge. When analyzing design that is not clearly spelled out in codes and standards such as the case of multilayered pressure vessel, analytical method and numerical method are commonly used to verify the design. As the number of layer increases, analyzing the multilayered vessel wall through analytical mean is more efficient as compared to numerical

mean (Chen and Ding, 2001). Among published literatures that have presented different analytical methods used to analyze multilayered structure, Shi et al. (2007), Vedeld and Sollund (2014) and Yeo et al. (2017) reported that analytical solution based on recursive algorithm is simple and efficient in solving thermo-mechanical problem of multilayered structure. The recent work by Yeo et al. (2017) derived the analytical solution based on recursive algorithm to obtain stresses and displacement of multilayered cylinder under plane strain assumption. It is not suitable to be applied in solving multilayered cylindrical pressure vessel problem because the axial strain induced by the closed end of cylindrical pressure vessel is significant (Wang et al., 2012). Also, there is no any literature that has presented the analytical solution to solve thermo-mechanical problem of multilayered spherical pressure vessel.

CHAPTER 3

METHODOLOGY

3.1. Introduction

The derivation of the proposed analytical solutions is outlined in Figure 3.1. First of all, the key assumptions, geometrical illustration, material properties, notations, boundary conditions and interface conditions that applied throughout the derivation for both cases of multilayered cylindrical and spherical pressure vessels are stated in Section 3.2 to Section 3.4. Subsequently, the analytical solution to obtain the temperature distribution across the vessel's wall for cylindrical multilayered pressure vessel is derived in Section 3.5. Section 3.6 presents the derivation of analytical solution that uses the obtained temperature distribution to identify radial, tangential and axial stresses across the vessel's wall. Next, a computational procedure that summarizes the sequence of unknowns and terms being computed is given in Section 3.7. Similarly, the derivation of analytical solution and computational procedure for spherical multilayered pressure vessel are expressed in Section 3.8 to Section 3.10.

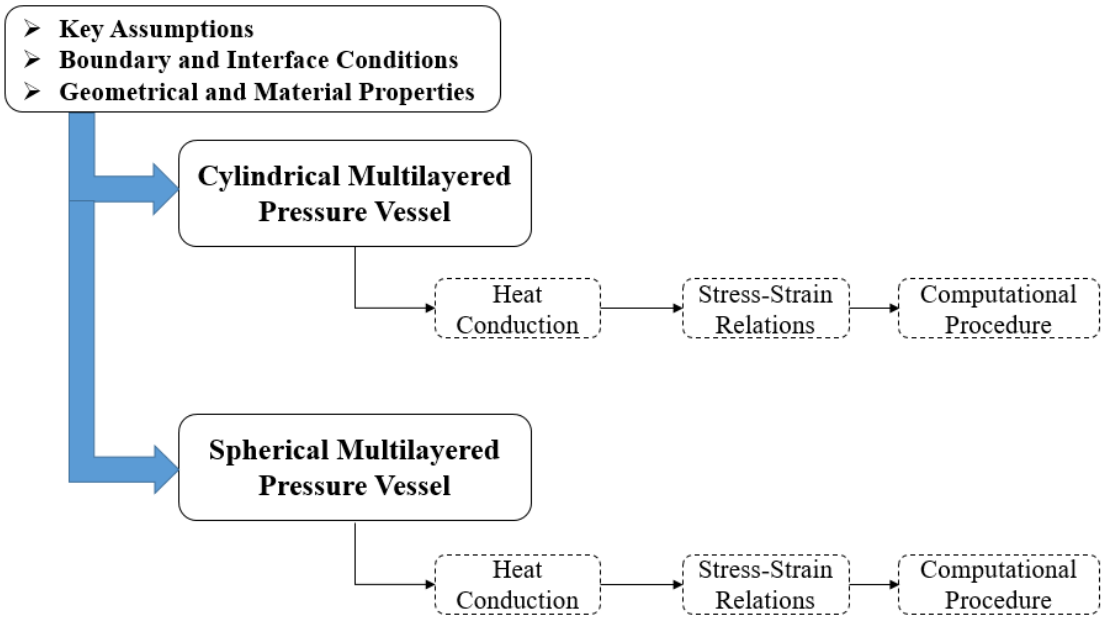

Figure 3.1: Sequence of the derivation of the proposed analytical solutions

3.2. Key Assumptions

The key assumptions applied throughout the derivation of the analytical solution are presented below:

1. The material properties across a same layer is homogenous.
2. The thermal and mechanical loadings on the vessel's wall are uniform and in steady state.
3. The heat transfer and stresses induced across the vessel's wall are axisymmetric.
4. Changes of dimension due to stress has negligible effect on heat transfer.
5. All layers are perfectly bonded.
6. The stress-strain relations for pressure vessel are derived based on small displacement condition.
7. The cylindrical pressure vessel wall's section experienced uniform axial

strain and taken to be under generalized plane strain condition.

3.3. Geometry, Material Properties and Loadings

Figure 3.2 and Figure 3.3 show the cross section view of a multilayered cylindrical and spherical pressure vessels respectively. The multilayered structure has n-number of layers where it is subjected to internal and external pressure and temperature loading. P_{int} and $\bar{T}_{int}$ is the pressure and temperature at inner surface, r_0 while P_{ext} and $\bar{T}_{ext}$ is the pressure and temperature on the outer surface, r_n. For any i-th layer, the outer radius is r_i while the material properties for i-th layer such as elastic modulus, Poisson's ratio, thermal expansion coefficient and thermal conductivity are E_i , ν_i , α_i and k_i respectively as depicted in Figure 3.2 and Figure 3.3.

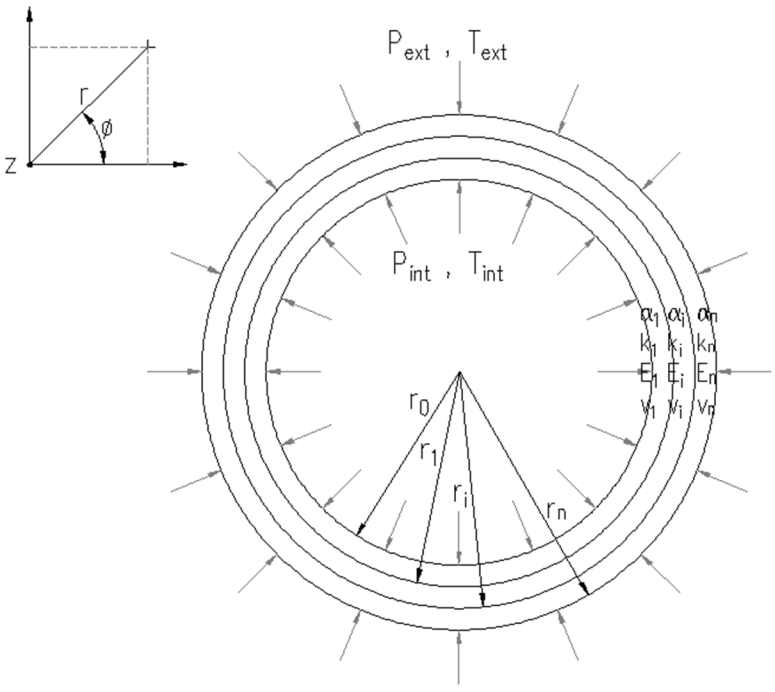

Figure 3.2: Section view of a multilayered cylindrical pressure vessel that is

subjected to temperature and pressure loading on inner and outer surface.

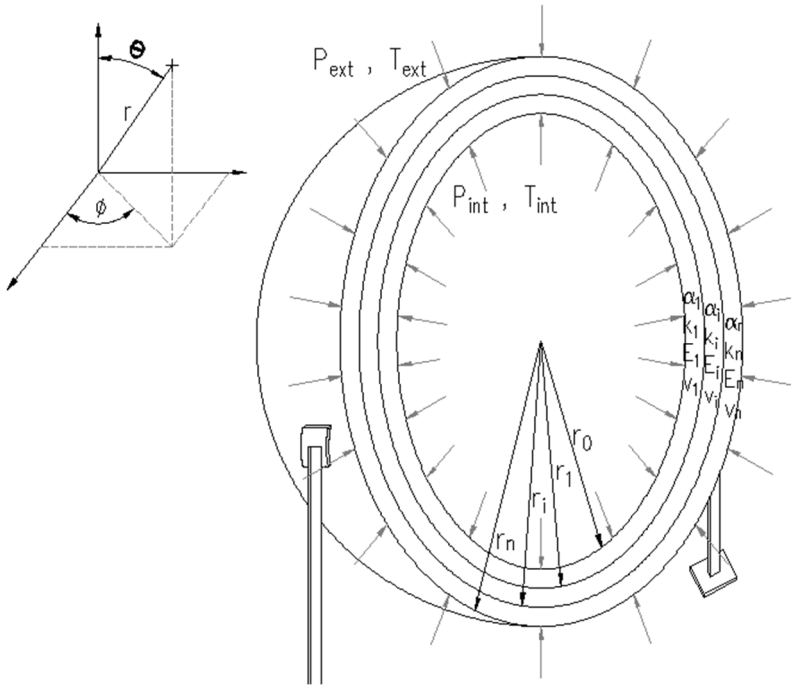

Figure 3.3: Section view of a multilayered spherical pressure vessel that is subjected to temperature and pressure loading on inner and outer surface.

3.4. Boundary and Interface Conditions

The boundary conditions on the inner surface are given as

$$T_1(r_0) = \bar{T}_0 = T_{int} \tag{3.1}$$

$$\sigma_{rr,1}(r_0) = -p_o = -P_{int} \tag{3.2}$$

where $T_1(r_0)$ represents the temperature of inner surface of first layer which is the temperature at radius r_0 written as $\bar{T}_0$. $\sigma_{rr,1}(r_0)$ denotes the compressive radial stress on the inner surface of first layer which is the pressure on radius r_0

written as $-p_0$. For the outer surface, the boundary conditions are given as

$$T_n(r_n) = \bar{T}_n = T_{ext} \tag{3.3}$$

$$\sigma_{rr,n}(r_n) = -p_n = -P_{ext} \tag{3.4}$$

where $T_n(r_n)$ represents the temperature of outer surface of nth layer which is the temperature at radius r_n written as $\bar{T}_n$. $\sigma_{rr,n}(r_n)$ denotes the compressive radial stress on the outer surface of nth layer which is the pressure on radius r_n written as $-p_n$.

At each interface layer, the continuity equations are such that

$$T_i(r_i) = T_{i+1}(r_i) \tag{3.5}$$

$$q''_i(r_i) = q''_{i+1}(r_i) \tag{3.6}$$

$$\sigma_{rr,i}(r_i) = \sigma_{rr,i+1}(r_i) \tag{3.7}$$

$$u_{r,i}(r_i) = u_{r,i+1}(r_i) \tag{3.8}$$

3.5. Heat Conduction for Multilayered Cylindrical Pressure Vessel

In this case, there is no energy generation within the structure and the heat transfer scenario can be simplified to one-dimensional steady state problem. Therefore, Eq. (2.7) can be reduced to

$$\frac{d}{dr}\left[r\frac{dT_i(r)}{dr}\right] = 0 \tag{3.9}$$

Integrating Eq. (3.9),

$$T_i(r) = A_i + B_i \ln r \tag{3.10}$$

The heat flux equation can be written as

$$q_i''(r) = -k_i \frac{dT_i(r)}{dr}$$

$$q_i''(r) = -k_i \frac{B_i}{r} \tag{3.11}$$

In order to get the temperature distribution across any layer i, the integration constants A_i and B_i need to be identified by using the boundary and interface conditions. By substituting Eq. (3.10) into Eq. (3.5)

$$A_i + B_i \ln r_i = A_{i+1} + B_{i+1} \ln r_i \tag{3.12}$$

Similarly, by using Eq. (3.6) and Eq. (3.11)

$$-k_i \left(\frac{B_i}{r_i}\right) = -k_{i+1} \left(\frac{B_{i+1}}{r_i}\right) \tag{3.13}$$

Rewriting Eq. (3.13) and Eq. (3.12)

$$A_{i+1} = A_i + B_i \ln r_i \left(1 - \frac{k_i}{k_{i+1}}\right) \tag{3.14}$$

$$B_{i+1} = B_i \left(\frac{k_i}{k_{i+1}} \right) \tag{3.15}$$

Writing inner and outer interface temperatures of two adjacent layers

$$A_i + B_i \ln r_{i-1} = \bar{T}_{i-1} \tag{3.16}$$

$$A_{i+1} + B_{i+1} \ln r_{i+1} = \bar{T}_{i+1} \tag{3.17}$$

Hence, by substituting Eq. (3.14) and Eq. (3.15) into Eq. (3.16) and Eq. (3.17), A_i and B_i can be

$$A_i = \frac{\bar{T}_{i+1} x_i - \bar{T}_{i-1} y_i}{x_i - y_i} \tag{3.18}$$

$$B_i = \frac{x_i (\bar{T}_{i-1} - \bar{T}_{i+1})}{\ln r_{i-1} (x_i - y_i)} \tag{3.19}$$

where

$$x_i = \delta_i \delta_{i+1} \tag{3.20}$$

$$y_i = \delta_{i+1} - \frac{k_i}{k_{i+1}} (\delta_{i+1} - 1) \tag{3.21}$$

$$\delta_i = \frac{\ln r_{i-1}}{\ln r_i} \tag{3.22}$$

The temperature at outer radius of layer i is

$$T_i(r_i) = A_i + B_i \ln r_i = \bar{T}_i \tag{3.23}$$

Putting Eq. (3.18) and Eq. (3.19) into Eq. (3.23) to obtain the relationship between temperatures at adjacent layers

$$\bar{T}_{i+1} = \frac{\bar{T}_{i-1}(\delta_i y_i - x_i) + \bar{T}_i \delta_i (x_i - y_i)}{x_i(\delta_i - 1)} \tag{3.24}$$

Hence, for any layer i, constant A_i and B_i can be written in terms of inner and outer temperatures of the layer by using Eq. (3.18) and Eq. (3.19)

$$A_i = \frac{\bar{T}_i \delta_i - \bar{T}_{i-1}}{\delta_i - 1} \tag{3.25}$$

$$B_i = \frac{\delta_i(\bar{T}_{i-1} - \bar{T}_i)}{\ln r_{i-1}\,(\delta_i - 1)} \tag{3.26}$$

To determine A_i and B_i, it is necessary to write $\bar{T}_i$ in terms of defined boundary values $\bar{T}_0$ and $\bar{T}_n$. Introducing two simple recurrence relations

$$a_{i+1} = \frac{a_{i-1}(\delta_i y_i - x_i) + a_i \delta_i (x_i - y_i)}{x_i(\delta_i - 1)} \tag{3.27}$$

$$b_{i+1} = \frac{b_{i-1}(\delta_i y_i - x_i) + b_i \delta_i (x_i - y_i)}{x_i(\delta_i - 1)} \tag{3.28}$$

where $i = 1,2,3 \ldots (n-1)$

Next, temperature $\bar{T}_i$ can be related to recurrence coefficients a and b as

$$\bar{T}_i = a_i \bar{T}_1 + b_i \bar{T}_0 \tag{3.29}$$

For the relation Eq. (3.29) to be valid, initial values of

$$a_0 = 0, a_1 = 1, b_0 = 1, b_1 = 0 \tag{3.30}$$

When $i = n$, $\bar{T}_1$ can be found through Eq. (3.31) and subsequently temperature i at all layer interfaces through Eq. (3.32)

$$\bar{T}_1 = \frac{\bar{T}_n - b_n \bar{T}_0}{a_n} \tag{3.31}$$

$$\bar{T}_i = \frac{a_i}{a_n} \bar{T}_n + \left(b_i - \frac{b_n}{a_n} a_i \right) \bar{T}_0 \tag{3.32}$$

By using temperature i at all layer interfaces, constants A_i and B_i can be identified. Hence, the temperature at each radius point can be found by using Eq. (3.10).

3.6. Stress-Strain Relations for Multilayered Cylindrical Pressure Vessel

The axisymmetric multilayered hollow cylinder section shown in Figure 3.2 has varying temperature in radial direction with $\Delta_i = T_i - T_r$ for T_r being the material initial temperature. Under small displacement and generalized plane strain conditions, the strain-displacement relations are (Boresi and Schmidt, 2009)

$$\epsilon_{rr,i} = \frac{du_{r,i}}{dr} \tag{3.33}$$

$$\epsilon_{\emptyset\emptyset,i} = \frac{u_{r,i}}{r} \tag{3.34}$$

$$\epsilon_{zz,i} = \frac{du_z}{dz} = C_z = constant \tag{3.35}$$

$$\epsilon_{r\emptyset,i} = \epsilon_{rz,i} = \epsilon_{\emptyset z,i} = 0 \tag{3.36}$$

$$\sigma_{rr,i} = \frac{E_i}{(1+v_i)(1-2v_i)}[(1-v_i)\epsilon_{rr,i} + v_i(\epsilon_{\emptyset\emptyset,i} + \epsilon_{zz,i}) - (1+v_i)\alpha_i\Delta_i] \tag{3.37}$$

$$\sigma_{\emptyset\emptyset,i} = \frac{E_i}{(1+v_i)(1-2v_i)}[(1-v_i)\epsilon_{\emptyset\emptyset,i} + v_i(\epsilon_{rr,i} + \epsilon_{zz,i}) - (1+v_i)\alpha_i\Delta_i] \tag{3.38}$$

$$\sigma_{zz,i} = \frac{E_i}{(1+v_i)(1-2v_i)}[v_i\left(\epsilon_{\emptyset\emptyset,i} + \epsilon_{rr,i}\right) + (1-v_i)\epsilon_{zz,i} - (1+v_i)\alpha_i\Delta_i] \tag{3.39}$$

The body force components B_x, B_y and B_z can be neglected and the load case is uniform and axisymmetric. Therefore, the non-trivial Eq. (2.47) can be reduced to

$$\frac{d\sigma_{rr,i}}{dr} + \frac{\sigma_{rr,i} - \sigma_{\emptyset\emptyset,i}}{r} = 0 \tag{3.40}$$

Using Eq. (3.33), Eq. (3.34), Eq. (3.35), Eq. (3.37) and Eq. (3.38), the equilibrium Eq. (3.40) can be written in terms of radial displacement

$$\frac{d}{dr}\left[\frac{1}{r}\frac{d\left(u_{r,i}r\right)}{dr}\right] = \frac{1+v_i}{1-v_i}\alpha_i\frac{d\Delta_i}{dr} \tag{3.41}$$

Integrating Eq. (3.41) to get radial displacement equation,

$$u_{r,i}(r) = \beta_i C_i r + \lambda_i \frac{(D_i + I_i)}{r} \tag{3.42}$$

where $C_i = \frac{\hat{C}}{\beta_i}$, $D_i = \frac{\widehat{D}}{\lambda_i}$ for $\hat{C}$ and $\widehat{D}$ are the integration constants and

$$I_i = -\frac{E_i \alpha_i}{1 - v_i} \int_{r_{i-1}}^{r} \Delta_i \, r dr \tag{3.43}$$

$$\beta_i = \frac{(1 + v_i)(1 - 2v_i)}{E_i} \tag{3.44}$$

$$\lambda_i = -\frac{(1 + v_i)}{E_i} \tag{3.45}$$

By substituting Eq. (3.33), Eq. (3.34), Eq. (3.35) and Eq. (3.42) in Eq. (3.37), Eq. (3.38) and Eq. (3.39), the equations for stresses have been written in terms of C_i and D_i

$$\sigma_{rr,i}(r) = C_i + \frac{D_i + I_i}{r^2} + \varphi_i \tag{3.46}$$

$$\sigma_{\emptyset\emptyset,i}(r) = C_i - \frac{D_i + I_i}{r^2} + \varphi_i - \frac{E_i \alpha_i \Delta_i}{(1 - v_i)} \tag{3.47}$$

$$\sigma_{zz,i}(r) = 2v_i C_i + \frac{E_i}{(1 + v_i)(1 - 2v_i)} (1 - v_i) \epsilon_{zz} - \frac{E_i \alpha_i \Delta_i}{(1 - v_i)} \tag{3.48}$$

where

$$\varphi_i = v_i \epsilon_{zz} / \beta_i \tag{3.49}$$

Therefore, by identifying C_i and D_i, the stresses and radial displacement throughout the multilayered cylindrical wall can be determined. By using Eq. (3.7) and Eq. (3.8)

$$C_i + \frac{D_i + I_i}{r_i^2} + \varphi_i = C_{i+1} + \frac{D_{i+1} + I_{i+1}^0}{r_i^2} + \varphi_{i+1} \tag{3.50}$$

$$\beta_i C_i r_i + \lambda_i \frac{(D_i + I_i)}{r_i} = \beta_{i+1} C_{i+1} r_i + \lambda_{i+1} \frac{(D_{i+1} + I_{i+1}^0)}{r_i} \tag{3.51}$$

where the thermal stress term $I_{i+1}^0 = I_{i+1}(r_i) = -\frac{E_{i+1}\alpha_{i+1}}{1-v_{i+1}} \int_{r_i}^{r_i} \Delta_i \, r dr = 0$

Rearranging Eq. (3.50) and Eq. (3.51), C_{i+1} and D_{i+1} can be written in terms of C_i and D_i

$$D_{i+1} = (D_i + I_i)\left(\frac{\lambda_i - \beta_{i+1}}{\lambda_{i+1} - \beta_{i+1}}\right) + C_i r_i^2 \left(\frac{\beta_i - \beta_{i+1}}{\lambda_{i+1} - \beta_{i+1}}\right) + \beta_{i+1} r_i^2 \left(\frac{\varphi_{i+1} - \varphi_i}{\lambda_{i+1} - \beta_{i+1}}\right) \tag{3.52}$$

$$C_{i+1} = \left(\frac{D_i + I_i}{r_i^2}\right)\left(\frac{\lambda_{i+1} - \lambda_i}{\lambda_{i+1} - \beta_{i+1}}\right) + C_i \left(\frac{\lambda_{i+1} - \beta_i}{\lambda_{i+1} - \beta_{i+1}}\right) + \lambda_{i+1} \left(\frac{\varphi_i - \varphi_{i+1}}{\lambda_{i+1} - \beta_{i+1}}\right) \tag{3.53}$$

Radial stresses at the inner and outer surface of two adjacent layers have been represented as the contact pressure

$$\sigma_{rr,i}(r_{i-1}) = -p_{i-1} => C_i + \frac{D_i + I_i^0}{r_{i-1}^2} + \varphi_i = -p_{i-1} \tag{3.54}$$

$$\sigma_{rr,i+1}(r_{i+1}) = -p_{i+1} => C_{i+1} + \frac{D_{i+1} + I_{i+1}}{r_{i+1}^2} + \varphi_{i+1} \tag{3.55}$$

$$= -p_{i+1}$$

for $I_i^0 = I_i(r_{i-1}) = -\frac{E_i \alpha_i}{1-v_i} \int_{r_{i-1}}^{r_{i-1}} \Delta_i \, r dr = 0$

Substituting Eq. (3.54) and Eq. (3.55) into Eq. (3.52) and Eq. (3.53) yields

$$D_i \tag{3.56}$$
$$= \gamma_i r_i^2 \left(\frac{p_{i-1} G_i - p_{i+1}(\lambda_{i+1} - \beta_{i+1}) + \varphi_i (G_i + \beta_{i+1}\gamma_{i+1} - \lambda_{i+1}) - \varphi_{i+1}\beta_{i+1}(\gamma_{i+1} - 1)}{S_i - G_i} \right)$$
$$- \frac{I_i S_i + I_{i+1}\gamma_i \gamma_{i+1}(\lambda_{i+1} - \beta_{i+1})}{S_i - G_i}$$

$$C_i = \frac{-p_{i-1} S_i + p_{i+1}(\lambda_{i+1} - \beta_{i+1}) - \varphi_i (S_i + \beta_{i+1}\gamma_{i+1} - \lambda_{i+1}) + \varphi_{i+1}\beta_{i+1}(\gamma_{i+1} - 1)}{S_i - G_i} \tag{3.57}$$
$$+ \frac{I_i S_i + I_{i+1}\gamma_i \gamma_{i+1}(\lambda_{i+1} - \beta_{i+1})}{r_{i-1}^2 (S_i - G_i)}$$

where

$$S_i = \gamma_i \gamma_{i+1}(\lambda_i - \beta_{i+1}) + (\lambda_{i+1} - \lambda_i)\gamma_i \tag{3.58}$$

$$G_i = \lambda_{i+1} - \beta_i + (\beta_i - \beta_{i+1})\gamma_{i+1} \tag{3.59}$$

$$\gamma_{i+1} = \frac{r_i^2}{r_{i+1}^2} \tag{3.60}$$

At the outer surface of layer i, the radial stress or contact pressure is

$$\sigma_{rr,i}(r_i) = -p_i \Rightarrow C_i + \frac{D_i + I_i}{r_i^2} + \varphi_i = -p_i \tag{3.61}$$

Substituting Eq. (3.56) and Eq. (3.57) into Eq. (3.61), the relation between contact pressures at adjacent layer is found

$$\begin{aligned} & p_{i+1} \\ & = \frac{p_{i-1}(S_i - \gamma_i G_i) - p_i(S_i - G_i)}{(1-\gamma_i)(\lambda_{i+1} - \beta_{i+1})} \\ & - \frac{I_{i+1}\gamma_{i+1}(\lambda_{i+1} - \beta_{i+1})(1-\gamma_i) + I_i\left({}^{S_i}/_{\gamma_i} - G_i\right)}{r_i^2(1-\gamma_i)(S_i - G_i)} \\ & - \frac{(1-\gamma_{i+1})(v_i - v_{i+1})\epsilon_{zz}}{(\lambda_{i+1} - \beta_{i+1})} \end{aligned} \tag{3.62}$$

Next, substituting Eq. (3.62) into Eq. (3.56) and Eq. (3.57) gives constant C_i and D_i for layer i in terms of its own inner and outer surface contact pressures

$$D_i = \frac{\gamma_i r_i^2}{1-\gamma_i}\left(p_i - p_{i-1} + \frac{I_i}{r_i^2}\right) \tag{3.63}$$

$$C_i = \frac{1}{1-\gamma_i}\left(\gamma_i p_{i-1} - p_i - \frac{I_i}{r_i^2}\right) - \varphi_i \tag{3.64}$$

To solve C_i and D_i, the constants need to be related to the known boundary values of p_0 and p_n. Two recurrence relations have been proposed

$$c_{i+1} = \frac{c_{i-1}(S_i - \gamma_i G_i) - c_i(S_i - G_i)}{(1-\gamma_i)(\lambda_{i+1} - \beta_{i+1})} \tag{3.65}$$

$$d_{i+1} \tag{3.66}$$

$$= \frac{d_{i-1}(S_i - \gamma_i G_i) - d_i(S_i - G_i)}{(1-\gamma_i)(\lambda_{i+1} - \beta_{i+1})}$$

$$- \frac{I_{i+1}\gamma_{i+1}(\lambda_{i+1} - \beta_{i+1})(1-\gamma_i) + I_i\left({}^{S_i}/_{\gamma_i} - G_i\right)}{p_0 r_i^2 (1-\gamma_i)(S_i - G_i)}$$

$$- \frac{(1-\gamma_{i+1})(v_i - v_{i+1})\epsilon_{zz}}{p_0(\lambda_{i+1} - \beta_{i+1})}$$

where $i = 1,2,3 \ldots (n-1)$

Introducing p_i in terms of recurrence coefficient c_i and d_i,

$$p_i = c_i p_1 + d_i p_0 \tag{3.67}$$

For Eq. (3.67) to be valid, initial values of c_i and d_i are

$$c_0 = 0, c_1 = 1, d_0 = 1, d_1 = 0 \tag{3.68}$$

For $i = n$,

$$p_1 = \frac{p_n - d_n p_0}{c_n} \tag{3.69}$$

Thus, p_i at all interfaces can be found through

$$p_i = \frac{c_i}{c_n} p_n + \left(d_i - \frac{d_n}{c_n} c_i \right) p_0 \tag{3.70}$$

However, ϵ_{zz} need to be identified to obtain the recurrence coefficient c_i and d_i. Eq. (3.66) has been separated into two terms to isolate the unknown ϵ_{zz}

$$d_i = e_i + f_i \epsilon_{zz} \tag{3.71}$$

for e_i and f_i to be

$$e_{i+1} \tag{3.72}$$
$$= \frac{e_{i-1}(S_i - \gamma_i G_i) - e_i(S_i - G_i)}{(1-\gamma_i)(\lambda_{i+1} - \beta_{i+1})}$$
$$- \frac{I_{i+1}\gamma_{i+1}(\lambda_{i+1} - \beta_{i+1})(1-\gamma_i) + I_i \left({S_i}/{\gamma_i} - G_i \right)}{p_0 r_i^2 (1-\gamma_i)(S_i - G_i)}$$

$$f_{i+1} = \frac{f_{i-1}(S_i - \gamma_i G_i) - f_i(S_i - G_i)}{(1-\gamma_i)(\lambda_{i+1} - \beta_{i+1})} \tag{3.73}$$
$$- \frac{(1-\gamma_{i+1})(v_i - v_{i+1})}{p_0(\lambda_{i+1} - \beta_{i+1})}$$

Using initial value

$$e_0 = 1, e_1 = 0, f_0 = 0, f_1 = 1 \tag{3.74}$$

Therefore, Eq. (3.70) can be modified into

$$p_i = \frac{c_i}{c_n} p_n + \left(e_i - \frac{e_n}{c_n} c_i\right) p_0 + \left(f_i - \frac{f_n}{c_n} c_i\right) p_0 \epsilon_{zz} \tag{3.75}$$

For the generalized plane strain case that can describe the scenario of a loaded closed end cylindrical pressure vessel, using Eq. (3.48) and Eq. (3.64) the ϵ_{zz} is such that

$$P_{ext}(\pi {r_n}^2) + \sum_{i=1}^{n} \int_{r_{i-1}}^{r_i} \sigma_{zz,i} \, [2\pi r] dr = P_{int}(\pi {r_0}^2) \tag{3.76}$$

$$\epsilon_{zz} = \frac{\chi_1}{\chi_2} \tag{3.77}$$

where

$$\begin{aligned} \chi_1 = {} & \frac{P_{int}(\pi {r_0}^2) - P_{ext}(\pi {r_n}^2)}{2\pi} \\ & - \sum_{i=1}^{n} \left\{ \frac{2v_i}{1-\gamma_i} \left(\gamma_i p_{i-1}^o - p_i^o \right. \right. \\ & \left. - \frac{I_i}{r_i^2} \right) \left[\frac{{r_i}^2 - {r_{i-1}}^2}{2} \right] + \frac{E_i \alpha_i T_r}{(1-v_i)} \left[\frac{{r_i}^2 - {r_{i-1}}^2}{2} \right] \\ & - \frac{E_i \alpha_i A_i}{(1-v_i)} \left[\frac{{r_i}^2 - {r_{i-1}}^2}{2} \right] \\ & - \frac{E_i \alpha_i B_i}{(1-v_i)} \left[\frac{{r_i}^2 \ln r_i}{2} - \frac{{r_i}^2}{4} \right. \\ & \left. \left. - \left(\frac{{r_{i-1}}^2 \ln r_{i-1}}{2} - \frac{{r_{i-1}}^2}{4} \right) \right] \right\} \end{aligned} \tag{3.78}$$

$$\chi_2 = \sum_{i=1}^{n} \left[\frac{2v_i}{1-\gamma_i} (\gamma_i \omega_{i-1} - \omega_i) + \frac{E_i}{(1+v_i)(1-2v_i)} (1-v_i) - \frac{2{v_i}^2}{\beta_i} \right] \left[\frac{{r_i}^2 - {r_{i-1}}^2}{2} \right] \tag{3.79}$$

for

$$p_i^o = \frac{c_i}{c_n} p_n + \left(e_i - \frac{e_n}{c_n} c_i \right) p_0 \tag{3.80}$$

$$\omega_i = \left(f_i - \frac{f_n}{c_n} c_i \right) p_0 \tag{3.81}$$

Hence, p_i at all interfaces can be identified. C_i and D_i can thus be found to get the stress distribution equation for all points.

3.7. Computational Procedure for Multilayered Cylindrical Pressure Vessel

The process of obtaining the temperature and stresses distribution across the multilayered cylindrical pressure vessel has been articulated in Section 3.5 and Section 3.6. The computational procedure can be written as below.

1) Determine the sequences of $\{x_i\}$, $\{y_i\}$ and $\{\delta_i\}$ following Eq. (3.20) to Eq. (3.22).
2) Compute the sequences $\{a_i\}$ and $\{b_i\}$ by using Eq. (3.27) and Eq. (3.28) with initial values from Eq. (3.30).

3) Identify sequences of $\{\bar{T}_i\}$ by using Eq. (3.32).

4) Calculate sequences of $\{A_i\}$ and $\{B_i\}$ by using Eq. (3.25) and Eq. (3.26).

5) Hence, temperature distribution can be obtained through Eq. (3.10). Sequences $\{\Delta_i\}$ is thus known.

6) Establish the sequences of $\{I_i\}$, $\{\beta_i\}$ and $\{\lambda_i\}$ following Eq. (3.43), Eq. (3.44) and Eq. (3.45).

7) Determine the sequences of $\{S_i\}$, $\{G_i\}$ and $\{\gamma_i\}$ by working out Eq. (3.58) to Eq. (3.60).

8) Compute the sequences of $\{c_i\}$, $\{e_i\}$ and $\{f_i\}$ by using Eq. (3.65), Eq. (3.72) and Eq. (3.73) with initial values from Eq. (3.68) and Eq. (3.74).

9) Work the sequences of $\{p_i^o\}$ and $\{\omega_i\}$ by using Eq. (3.80) and Eq. (3.81).

10) Identify χ_1 and χ_2 by using Eq. (3.78) and Eq. (3.79).

11) Calculate ϵ_{zz} following Eq. (3.77).

12) Compute $\{p_i\}$ in Eq. (3.75) and $\{\varphi_i\}$ in Eq. (3.49).

13) After that, $\{D_i\}$ and $\{C_i\}$ can be obtained from Eq. (3.63) and Eq. (3.64). Lastly, stresses in Eq. (3.46) to Eq. (3.48) can be computed by using $\{C_i\}$ and $\{D_i\}$.

Figure 3.4 illustrates a computational procedure flow chart that shows the sequence of parameters being computed when the developed analytical solution is used to obtain stresses across the multilayered cylindrical vessel wall.

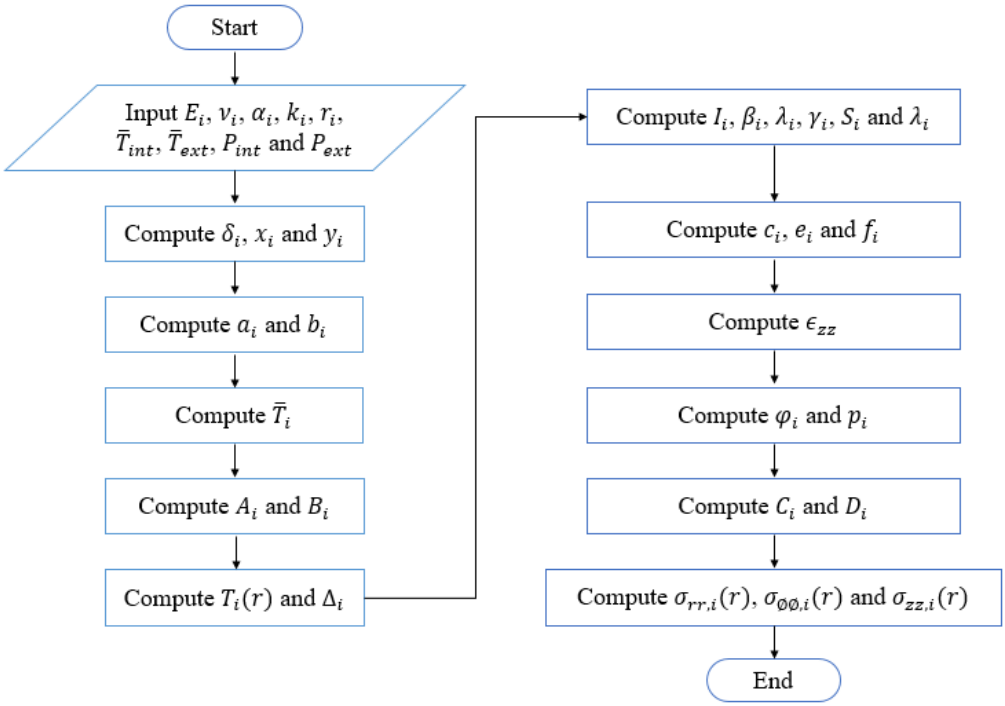

Figure 3.4: Flow chart of parameters being computed for multilayered cylindrical pressure vessel

3.8. Heat Conduction for Multilayered Spherical Pressure Vessel

Similar to the cylindrical pressure vessel, it is assumed that no energy generation within the pressure vessel's structure and the heat transfer scenario can be simplified to one-dimensional steady state problem. With reference to Eq. (2.8), the reduced equation is

$$\frac{d}{dr}\left[r^2\frac{dT_i(r)}{dr}\right] = 0 \tag{3.82}$$

Integrating Eq. (3.82),

$$T_i(r) = A_i - \frac{B_i}{r} \tag{3.83}$$

The heat flux for spherical structure can be written as

$$q_i^{"}(r) = -k\frac{dT_i(r)}{dr}$$

$$q_i^{"}(r) = -k\frac{B_i}{r^2} \tag{3.84}$$

In order to get the temperature distribution across any layer i, the integration constants A_i and B_i need to be identified by using the boundary and interface conditions. By substituting Eq. (3.83) into Eq. (3.5)

$$A_i - \frac{B_i}{r_i} = A_{i+1} - \frac{B_{i+1}}{r_i} \tag{3.85}$$

Similarly, by using Eq. (3.6) and Eq. (3.84),

$$k_i\left(\frac{B_i}{{r_i}^2}\right) = k_{i+1}\left(\frac{B_{i+1}}{{r_i}^2}\right) \tag{3.86}$$

Rewriting Eq. (3.85) and (3.86)

$$A_{i+1} = A_i + \frac{B_{i+1} - B_i}{r_i} \tag{3.87}$$

$$B_{i+1} = B_i \left(\frac{k_i}{k_{i+1}} \right) \tag{3.88}$$

Writing inner and outer interface temperatures of two adjacent layers

$$A_i + \frac{B_i}{r_{i-1}} = \bar{T}_{i-1} \tag{3.89}$$

$$A_{i+1} + \frac{B_{i+1}}{r_{i+1}} = \bar{T}_{i+1} \tag{3.90}$$

Hence, by substituting Eq. (3.87) and Eq. (3.88) into Eq. (3.89) and Eq. (3.90), A_i and B_i can be

$$A_i = \frac{\bar{T}_{i-1} x_i + \bar{T}_{i+1} y_i}{x_i + y_i} \tag{3.91}$$

$$B_i = \frac{\bar{T}_{i+1} - \bar{T}_{i-1}}{x_i + y_i} \tag{3.92}$$

where

$$x_i = \frac{1}{r_i} \left[\frac{k_i}{k_{i+1}} - 1 \right] - \frac{1}{r_{i+1}} \left[\frac{k_i}{k_{i+1}} \right] \tag{3.93}$$

$$y_i = \frac{1}{r_{i-1}} \tag{3.94}$$

The temperature at outer radius of layer i is

$$T_i(r_i) = A_i - \frac{B_i}{r_i} = \bar{T}_i \tag{3.95}$$

Putting Eq. (3.91) and Eq. (3.92) into Eq. (3.95) to obtain the relationship between temperatures at adjacent layers

$$\bar{T}_{i+1} = \frac{\bar{T}_i(x_i + y_i) - \bar{T}_{i-1}(x_i + y_{i+1})}{(y_i - y_{i+1})} \tag{3.96}$$

Therefore, for any layer i, constant A_i and B_i can be written in terms of inner and outer temperatures of the layer by using Eq. (3.91) and Eq. (3.92)

$$A_i = \frac{\bar{T}_i y_i - \bar{T}_{i-1} y_{i+1}}{(y_i - y_{i+1})} \tag{3.97}$$

$$B_i = \frac{\bar{T}_i - \bar{T}_{i-1}}{y_i - y_{i+1}} \tag{3.98}$$

To determine A_i and B_i, it is necessary to write $\bar{T}_i$ in terms of defined boundary values $\bar{T}_0$ and $\bar{T}_n$. Introducing two simple recurrence relations

$$a_{i+1} = \frac{a_i(x_i + y_i) - a_{i-1}(x_i + y_{i+1})}{(y_i - y_{i+1})} \tag{3.99}$$

$$b_{i+1} = \frac{b_i(x_i + y_i) - b_{i-1}(x_i + y_{i+1})}{(y_i - y_{i+1})} \tag{3.100}$$

where $i = 1,2,3 \ldots (n-1)$

Next, temperature $\bar{T}_i$ can be related to recurrence coefficients a and b as

$$\bar{T}_i = a_i \bar{T}_1 + b_i \bar{T}_0 \tag{3.101}$$

For the relation Eq. (3.101) to be valid, initial values need to be

$$a_0 = 0, a_1 = 1, b_0 = 1, b_1 = 0 \tag{3.102}$$

When $i = n$, $\bar{T}_1$ can be found through Eq. (3.103) and subsequently temperature i at all layer interfaces through Eq. (3.104)

$$\bar{T}_1 = \frac{\bar{T}_n - b_n \bar{T}_0}{a_n} \tag{3.103}$$

$$\bar{T}_i = \frac{a_i}{a_n} \bar{T}_n + \left(b_i - \frac{b_n}{a_n} a_i \right) \bar{T}_0 \tag{3.104}$$

By using temperature i at all layer interfaces, constants A_i and B_i can be identified. Hence, the temperature at each radius point can be found by using Eq. (3.83).

3.9. Stress-Strain Relations for Multilayered Spherical Pressure Vessel

The axisymmetric multilayered hollow sphere section shown in Figure 3.3 has varying temperature in radial direction with $\Delta_i = T_i - T_r$ for T_r being the material initial temperature. Under small displacement assumption, the strain-displacement relations are (Boresi and Schmidt, 2009)

$$\epsilon_{rr,i} = \frac{du_{r,i}}{dr} \tag{3.105}$$

$$\epsilon_{\emptyset\emptyset,i} = \frac{u_{r,i}}{r} \tag{3.106}$$

$$\epsilon_{\theta\theta,i} = \epsilon_{\emptyset\emptyset,i} \tag{3.107}$$

$$\epsilon_{r\theta,i} = \epsilon_{\theta\emptyset,i} = 0 \tag{3.108}$$

$$\sigma_{rr,i} = \frac{E_i}{(1-2\nu_i)(\nu_i+1)}\left[(1-\nu_i)\epsilon_{rr,i} + 2\nu_i\epsilon_{\emptyset\emptyset,i} - \alpha_i\Delta_i(\nu_i+1)\right] \tag{3.109}$$

$$\sigma_{\emptyset\emptyset,i} = \frac{E_i}{(1-2\nu_i)(\nu_i+1)}\left[\nu_i\epsilon_{rr,i} + \epsilon_{\emptyset\emptyset,i} - \alpha_i\Delta_i(\nu_i+1)\right] \tag{3.110}$$

$$\sigma_{\theta\theta,i} = \sigma_{\emptyset\emptyset,i} \tag{3.111}$$

The body force components B_x, B_y and B_z can be neglected and the load case is uniform and axisymmetric. Therefore, Eq. (2.56) to Eq. (2.58) can be reduced to variation in only radial direction

$$\frac{d\sigma_{rr,i}}{dr} + \frac{2\left(\sigma_{rr,i} - \sigma_{\emptyset\emptyset,i}\right)}{r} = 0 \tag{3.112}$$

Using Eq. (3.105), Eq. (3.106), Eq. (3.109) and Eq. (3.110), the equilibrium Eq. (3.112) can be written in terms of radial displacement

$$\frac{d}{dr}\left[\frac{1}{r^2}\frac{d(u_{r,i}r^2)}{dr}\right] = \frac{(1+\nu_i)}{(1-\nu_i)}\alpha_i\frac{d\Delta_i}{dr} \tag{3.113}$$

Integrating Eq. (3.113) to get radial displacement equation,

$$u_{r,i} = \beta_i \mathrm{C_i} r + \lambda_i \frac{D_i}{r^2} + \frac{1}{r^2}\frac{\lambda_i}{\varphi_i}\mathrm{I}_i \tag{3.114}$$

where $C_i = \frac{\hat{C}}{\beta_i}$, $D_i = \frac{\widehat{D}}{\lambda_i}$ for $\hat{C}$ and $\widehat{D}$ are the integration constants

$$I_i = \int_{r_{i-1}}^{r} \Delta_i \, r^2 dr \tag{3.115}$$

$$\beta_i = \frac{(1-2\nu_i)}{E_i} \tag{3.116}$$

$$\lambda_i = -\frac{(1+\nu_i)}{2E_i} \tag{3.117}$$

$$\varphi_i = -\frac{(1-\nu_i)}{2E_i\alpha_i} \tag{3.118}$$

By substituting Eq. (3.114), Eq. (3.105) and Eq. (3.106) into Eq. (3.109) and Eq. (3.110), the equations for stresses have been written in terms of C_i and D_i

$$\sigma_{rr,i} = \mathrm{C_i} + \frac{D_i}{r^3} + \frac{\mathrm{I}_i}{\varphi_i r^3} \tag{3.119}$$

$$\sigma_{\emptyset\emptyset,i} = \mathrm{C_i} - \frac{D_i}{2r^3} - \frac{\mathrm{I}_i}{2r^3\varphi_i} + \frac{\Delta_i}{2\varphi_i} \tag{3.120}$$

Therefore, by identifying C_i and D_i, the stresses and radial displacement throughout the multilayered spherical wall can be determined. By using Eq. (3.7) and Eq. (3.8)

$$\mathrm{C_i} + \frac{D_i}{{r_i}^3} + \frac{\mathrm{I}_i}{\varphi_i {r_i}^3} = \mathrm{C_{i+1}} + \frac{D_{i+1}}{{r_i}^3} + \frac{\mathrm{I}^0_{i+1}}{\varphi_i r^3} \tag{3.121}$$

$$\beta_i \mathrm{C_i} r_i + \lambda_i \frac{D_i}{{r_i}^2} + \frac{\lambda_i}{\varphi_i {r_i}^2}\mathrm{I}_i = \beta_{i+1}\mathrm{C_{i+1}} r_i + \lambda_{i+1}\frac{D_{i+1}}{{r_i}^2} + \frac{\lambda_{i+1}}{\varphi_{i+1}{r_i}^2}\mathrm{I}^0_{i+1} \tag{3.122}$$

The thermal stress term $\mathrm{I}^0_{i+1} = \mathrm{I}_{i+1}(r_i) = \int_{r_i}^{r_i} \Delta_i r^2 dr = 0$

Rearranging Eq. (3.121) and Eq. (3.122), C_{i+1} and D_{i+1} can be written in terms of C_i and D_i

$$D_{i+1} = \left[\frac{\beta_i - \beta_{i+1}}{\lambda_{i+1} - \beta_{i+1}}\right]\mathrm{C_i}{r_i}^3 + \left[\frac{\lambda_i - \beta_{i+1}}{\lambda_{i+1} - \beta_{i+1}}\right]D_i + \left[\frac{\lambda_i - \beta_{i+1}}{\varphi_i(\lambda_{i+1} - \beta_{i+1})}\right]\mathrm{I}_i \tag{3.123}$$

$$\mathrm{C_{i+1}} = \left[\frac{\lambda_{i+1} - \beta_i}{\lambda_{i+1} - \beta_{i+1}}\right]\mathrm{C_i} + \left[\frac{\lambda_{i+1} - \lambda_i}{(\lambda_{i+1} - \beta_{i+1}){r_i}^3}\right]D_i + \left[\frac{\lambda_{i+1} - \lambda_i}{\varphi_i(\lambda_{i+1} - \beta_{i+1}){r_i}^3}\right]\mathrm{I}_i \tag{3.124}$$

Radial stresses at the inner and outer surface of two adjacent layers have been represented as the contact pressure

$$\sigma_{rr,i}(r_{i-1}) = -p_{i-1} \Rightarrow \mathrm{C_i} + \frac{D_i}{{r_{i-1}}^3} + \frac{\mathrm{I}^0_i}{\varphi_i {r_{i-1}}^3} = -p_{i-1} \tag{3.125}$$

$$\sigma_{rr,i+1}(r_{i+1}) = -p_{i+1} => \mathrm{C_{i+1}} + \frac{D_{i+1}}{{r_{i+1}}^3} + \frac{\mathrm{I}_{i+1}}{\varphi_{i+1}{r_{i+1}}^3} \tag{3.126}$$

$$= -p_{i+1}$$

for $I_i^0 = I_i(r_{i-1}) = \int_{r_{i-1}}^{r_{i-1}} \Delta_i r^2 dr = 0$

Substituting Eq. (3.125) and Eq. (3.126) into Eq. (3.123) and Eq. (3.124) yields

$$D_i = {r_i}^3 \gamma_i \left[\frac{G_i p_{i-1} - (\lambda_{i+1} - \beta_{i+1})p_{i+1}}{(S_i - G_i)}\right] - \frac{S_i \mathrm{I}_i}{\varphi_i (S_i - G_i)} \tag{3.127}$$

$$- \frac{(\lambda_{i+1} - \beta_{i+1})\gamma_{i+1}\,\gamma_i \mathrm{I}_{i+1}}{\varphi_{i+1}(S_i - G_i)}$$

$$\mathrm{C_i} = \frac{(\lambda_{i+1} - \beta_{i+1})p_{i+1} - S_i p_{i-1}}{(S_i - G_i)} + \frac{S_i \mathrm{I}_i}{\varphi_i (S_i - G_i){r_{i-1}}^3} \tag{3.128}$$

$$+ \frac{(\lambda_{i+1} - \beta_{i+1})\mathrm{I}_{i+1}}{\varphi_{i+1}(S_i - G_i){r_{i+1}}^3}$$

where

$$S_i = \gamma_i \gamma_{i+1}(\lambda_i - \beta_{i+1}) + \gamma_i(\lambda_{i+1} - \lambda_i) \tag{3.129}$$

$$G_i = (\lambda_{i+1} - \beta_i) + \gamma_{i+1}(\beta_i - \beta_{i+1}) \tag{3.130}$$

$$\gamma_{i+1} = \frac{{r_i}^3}{{r_{i+1}}^3} \tag{3.131}$$

At the outer surface of layer i, the radial stress or contact pressure is

$$\sigma_{rr,i}(r_i) = -p_i \Rightarrow \mathrm{C_i} + \frac{D_i}{{r_i}^3} + \frac{\mathrm{I}_i}{\varphi_i {r_i}^3} = -p_i \tag{3.132}$$

Substituting Eq. (3.127) and Eq. (3.128) into Eq. (3.132), the relation between contact pressures at adjacent layers is found

$$\begin{aligned} p_{i+1} = {} & \frac{(S_i - \gamma_i G_i)}{(\lambda_{i+1} - \beta_{i+1})(1-\gamma_i)} p_{i-1} \\ & - \frac{(S_i - G_i)}{(\lambda_{i+1} - \beta_{i+1})(1-\gamma_i)} p_i - \frac{\mathrm{I}_{i+1}}{\varphi_{i+1} {r_{i+1}}^3} \\ & - \frac{(S_i - \gamma_i G_i)}{(\lambda_{i+1} - \beta_{i+1})(1-\gamma_i)\varphi_i {r_{i-1}}^3} \mathrm{I}_i \end{aligned} \tag{3.133}$$

Next, substituting Eq. (3.133) into Eq. (3.127) and Eq. (3.128) gives constant C_i and D_i for layer i in terms of its own inner and outer surface contact pressures

$$D_i = {r_i}^3 \gamma_i \left[\frac{p_i - p_{i-1}}{(1-\gamma_i)} + \frac{1}{(1-\gamma_i)\varphi_i {r_i}^3} \mathrm{I}_i \right] \tag{3.134}$$

$$C_i = \frac{\gamma_i p_{i-1} - p_i}{(1-\gamma_i)} - \frac{1}{\varphi_i (1-\gamma_i) {r_i}^3} \mathrm{I}_i \tag{3.135}$$

To solve C_i and D_i, the constants need to be related to the known boundary values of p_0 and p_n. Two recurrence relations have been proposed

$$c_{i+1} = \frac{(S_i - \gamma_i G_i)}{(\lambda_{i+1} - \beta_{i+1})(1-\gamma_i)} c_{i-1} - \frac{(S_i - G_i)}{(\lambda_{i+1} - \beta_{i+1})(1-\gamma_i)} c_i \tag{3.136}$$

$$d_{i+1} = \frac{(S_i - \gamma_i G_i)}{(\lambda_{i+1} - \beta_{i+1})(1-\gamma_i)} d_{i-1} - \frac{(S_i - G_i)}{(\lambda_{i+1} - \beta_{i+1})(1-\gamma_i)} d_i - \frac{I_{i+1}}{p_0 \varphi_{i+1} {r_{i+1}}^3} - \frac{(S_i - \gamma_i G_i)}{(\lambda_{i+1} - \beta_{i+1})(1-\gamma_i) p_0 \varphi_i {r_{i-1}}^3} I_i \tag{3.137}$$

where $i = 1,2,3 \ldots (n-1)$

Introducing p_i in terms of recurrence coefficient c_i and d_i,

$$p_i = c_i p_1 + d_i p_0 \tag{3.138}$$

For Eq. (3.138) to be valid, initial values of c_i and d_i are

$$c_0 = 0, c_1 = 1, d_0 = 1, d_1 = 0 \tag{3.139}$$

for $i = n$,

$$p_1 = \frac{p_n - d_n p_0}{c_n} \tag{3.140}$$

Thus, p_i at all interfaces can be found through

$$p_i = \frac{c_i}{c_n} p_n + \left(d_i - \frac{d_n}{c_n} c_i \right) p_0 \tag{3.141}$$

Hence, p_i at all interfaces can be identified. C_i and D_i can thus be found to get the stress distribution equation for all points.

3.10. Computational Procedure for Multilayered Spherical Pressure Vessel

Based on the derivation presented in Section 3.8 and Section 3.9, the thermo-mechanical stresses in spherical pressure vessel can be estimated based on the computational procedure stated below.

1) Work out the sequences of $\{x_i\}$ and $\{y_i\}$ following Eq. (3.93) and Eq. (3.94).
2) Compute the sequences $\{a_i\}$ and $\{b_i\}$ by using Eq. (3.99) and Eq. (3.100) with initial values from Eq. (3.102).
3) Identify sequences of $\{\bar{T}_i\}$ by using Eq. (3.104).
4) Calculate sequences of $\{A_i\}$ and $\{B_i\}$ by using Eq. (3.97) and Eq. (3.98).
5) Hence, temperature distribution can be obtained through Eq. (3.83). Sequences $\{\Delta_i\}$ is thus known.
6) Establish the sequences of $\{I_i\}$, $\{\beta_i\}$, $\{\lambda_i\}$ and $\{\varphi_i\}$ following Eq. (3.115) to Eq. (3.118).
7) Determine the sequences of $\{\gamma_i\}$, $\{G_i\}$ and $\{S_i\}$ by working out Eq. (3.129) to Eq. (3.131).
8) Compute the sequences of $\{c_i\}$ and $\{d_i\}$ by using Eq. (3.136) and Eq. (3.137) with initial values from Eq. (3.139).

9) Compute $\{p_i\}$ in Eq. (3.141).

10) After that, $\{C_i\}$ and $\{D_i\}$ can be obtained from Eq. (3.134) and Eq. (3.135).

11) Lastly, stresses in Eq. (3.119) and Eq. (3.120) can be computed by using $\{C_i\}$ and $\{D_i\}$.

Figure 3.5 illustrates a computational procedure flow chart that shows the sequence of parameters being computed when the developed analytical solution is used to obtain stresses across the multilayered spherical vessel wall.

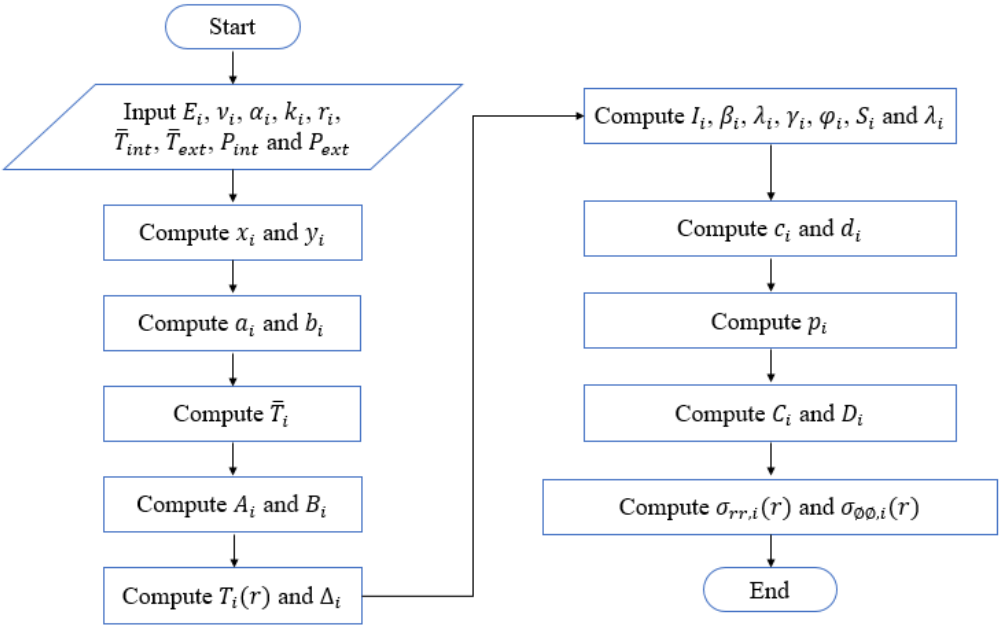

Figure 3.5: Flow chart of parameters being computed for multilayered spherical pressure vessel

CHAPTER 4

RESULTS AND DISCUSSION

4.1. Verification of Algorithm

The proposed analytical solutions to solve cylindrical and spherical multilayered pressure vessel problem are validated through comparison between results obtained by using the proposed recursive algorithm and ANSYS finite element method (FEM) simulation. The material and environment reference temperature was set to be 0 ℃. The simulation ran under two-dimensional, axisymmetric and steady state settings. The simulation started with heat analysis by using PLANE77 elements. After that, the obtained temperature distribution was transferred to structural module to simulate the thermal stress induced. Then, the structural simulation proceeded by using PLANE183 mechanical element to compute the stresses results.

4.1.1. Verification of Algorithm for Cylindrical Pressure Vessel

A six-layered cylindrical composite pressure vessel FEM model was adopted from the work of Zhang et al. (2012). The model was constructed and meshed into a total 54211 elements. The interfaces of adjacent layers were bonded to ensure mesh connectivity. The geometrical and material properties are shown in Table 4.1. The pressure and temperature applied at the inner

surface of the cylindrical composite pressure vessel are 200 °C and 22 MPa. The pressure and temperature applied at the outer surface of the cylindrical composite pressure vessel are 190 °C and 0.1 MPa.

Table 4.1: Geometry and material properties of cylindrical FEM model

Layers	Inner Radius, m	Outer Radius, m	E, Pa	v	$k, Wm^{-1}°C^{-1}$	$\alpha, °C^{-1}$
1	0.50	0.51	1.90×10^{11}	0.28	18.4	1.87×10^{-5}
2	0.51	0.52	1.94×10^{11}	0.28	25.4	1.74×10^{-5}
3	0.52	0.53	1.98×10^{11}	0.28	32.4	1.61×10^{-5}
4	0.53	0.54	2.02×10^{11}	0.28	39.4	1.48×10^{-5}
5	0.54	0.55	2.06×10^{11}	0.28	46.4	1.35×10^{-5}
6	0.55	0.58	2.10×10^{11}	0.3	53.4	1.22×10^{-5}

Figure 4.1 shows that the temperature distribution computed by using FEM and the proposed analytical solution agreed well with each other. The temperature profile experienced a gradual decline from internal boundary value to external boundary value across the vessel's wall.

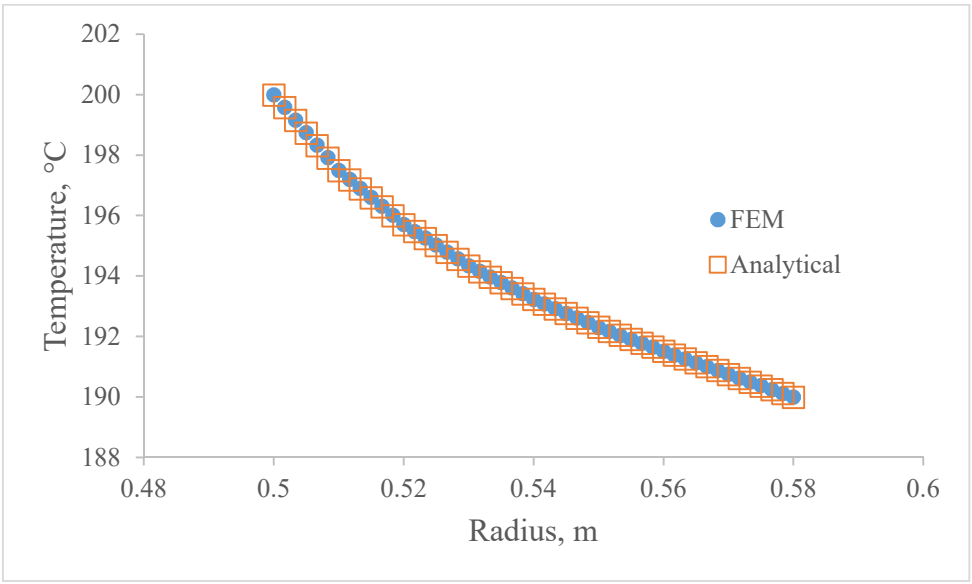

Figure 4.1: Temperature distribution across cylindrical vessel's wall

Figure 4.2 shows that the radial stresses computed by using proposed analytical solution and FEM are in good agreement. Inner and outer surfaces of the pressure vessel are not constrained in radial direction and thus the radial stress induced due to temperature change is zero at inner and outer surfaces. The vessel's wall experienced compressive stress because it is exposed to higher pressure and temperature at the inner surface.

Figure 4.3 and Figure 4.4 shows the tangential stress and axial stress across the vessel's wall. In general, the results produced from the proposed analytical solution are showing good agreement with FEM results. Similar to the work of Zhang et al. (2012) and Vedeld and Sollund (2014), the overall tangential and axial stresses exhibited discontinuity pattern at interface of different layers. In this case, the vessel experienced tensile mechanical stress in both tangential and axial direction because the vessel's structure is holding on to each other to contain the higher internal pressure. The thermal stress has contributed to the discontinuity of the overall stress. Typically, if the structure has smooth transition of material's thermal properties across different layers, it may help to reduce stresses discontinuity across the vessel's wall (Bhavar et al., 2017). The tangential and axial stresses due to mechanical loading recorded to be a consistent tensile stress across the vessel's wall while the tangential and axial stresses due to thermal loading shown a stepwise discontinuous stress from compression at inner surface to tension at outer surface of the vessel. Similarly, the stepwise discontinuous pattern is also observed from the overall tangential and axial stresses which is due to both mechanical and thermal loading.

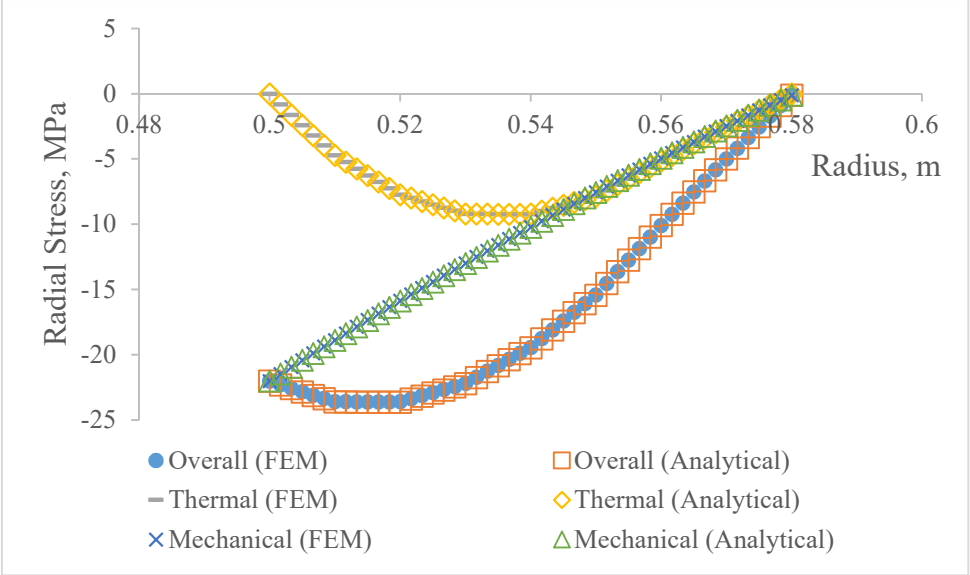

Figure 4.2: Radial stress across cylindrical vessel's wall

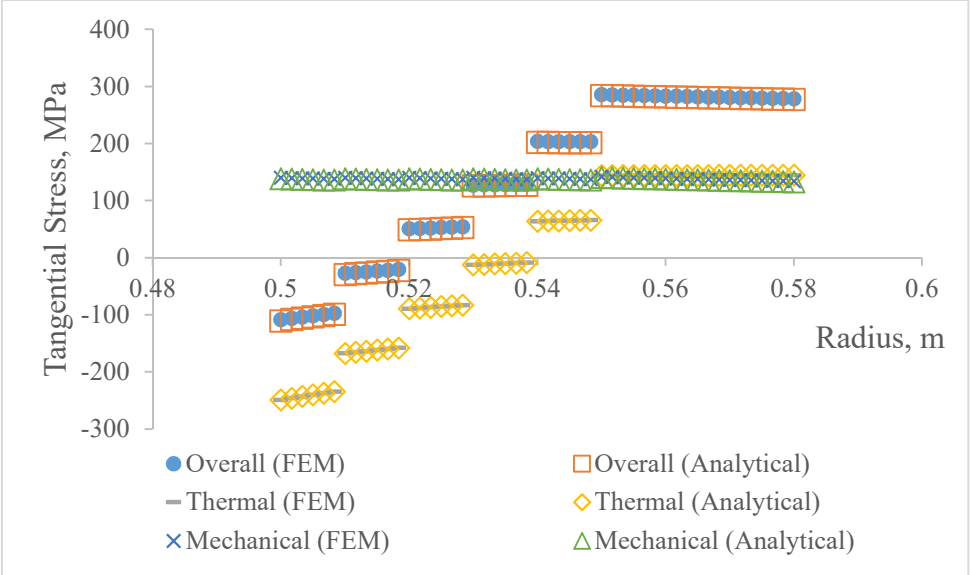

Figure 4.3: Tangential stress across cylindrical vessel's wall

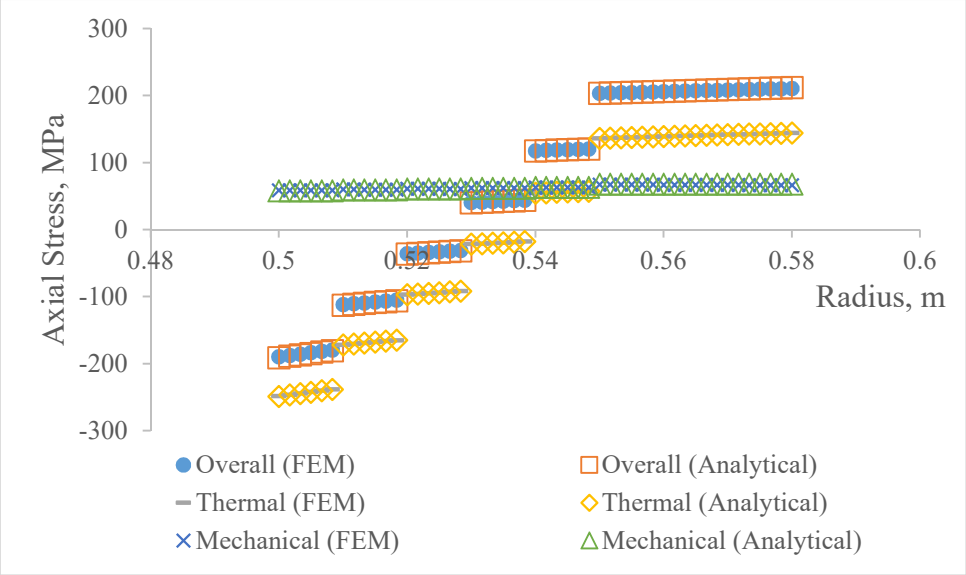

Figure 4.4: Axial stress across cylindrical vessel's wall

Figure 4.5 shows that the derived algorithm can also be used to predict stress response under plane strain assumption. Figure 4.5 exhibits the comparison of Von Mises stress for vessel described above under generalized plane strain and plane strain assumption. Von Mises yield criterion has been commonly used in predicting yielding of ductile metal (Boresi and Schmidt, 2009). It shows that Von Mises stress computed varies significantly when axial strain is taken into consideration. Therefore, axial strain plays an important role in evaluating the structural integrity of a pressure vessel.

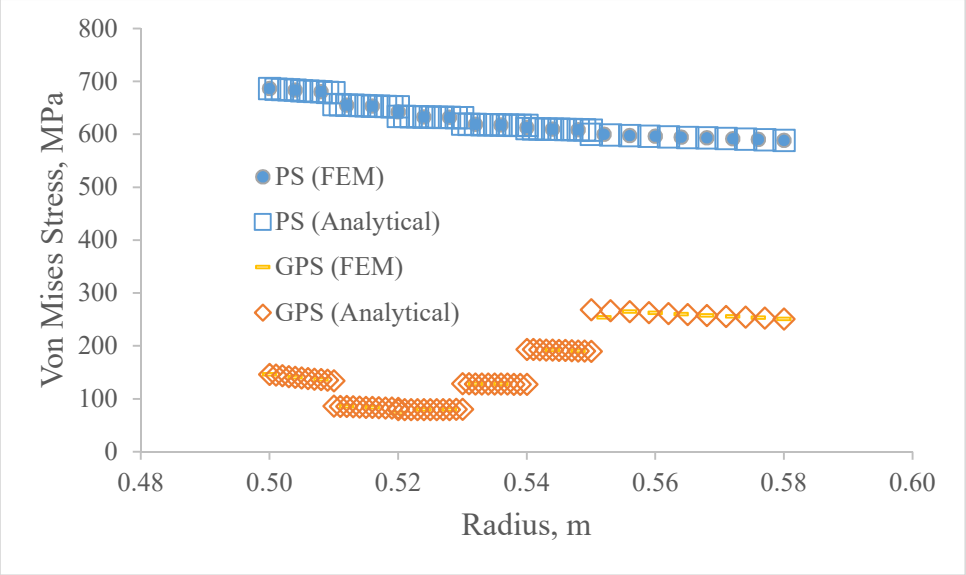

Figure 4.5: Comparison of the effect of generalized plane strain and plane strain assumptions to the Von Mises stress across cylindrical vessel's wall

4.1.2. Verification of Algorithm for Spherical Pressure Vessel

A five-layered spherical composite pressure vessel FEM model was constructed with reference to the work of Bayat et al. (2012). The model was meshed and generated total number of 71853 elements. The interfaces of adjacent layers were bonded to ensure mesh connectivity. The geometrical and material properties are shown in Table 4.2. The pressure and temperature applied at the inner surface of the cylindrical composite pressure vessel are 300 °C and 80 MPa. The pressure and temperature applied at the outer surface of the cylindrical composite pressure vessel are 25 °C and 0.1 MPa.

Table 4.2: Geometry and material properties of spherical FEM model

Layers	Inner Radius, m	Outer Radius, m	E, Pa	v	$k, Wm^{-1}°C^{-1}$	$\alpha, °C^{-1}$
1	0.04	0.044	2.21×10^{11}	0.3	55.2	1.324×10^{-6}
2	0.044	0.048	2.65×10^{11}	0.3	66.2	1.588×10^{-6}
3	0.048	0.052	3.13×10^{11}	0.3	78.2	1.876×10^{-6}
4	0.052	0.056	3.65×10^{11}	0.3	91.2	2.188×10^{-6}
5	0.056	0.06	4.21×10^{11}	0.3	105.2	2.524×10^{-6}

Figure 4.6 shows that the temperature distribution computed by using FEM and the proposed analytical solution matched perfectly with each other. The temperature profile experienced a gradual decline from internal boundary value to external boundary value.

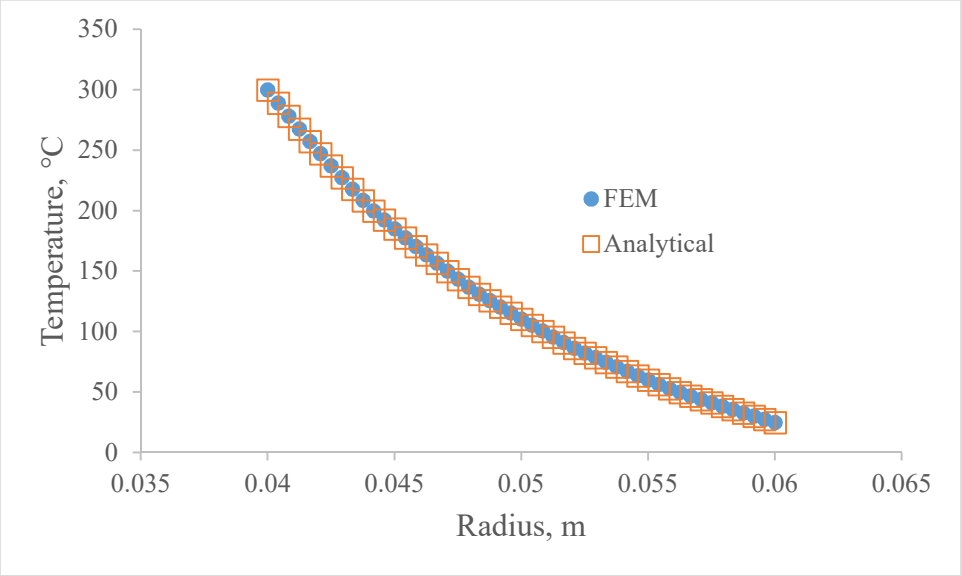

Figure 4.6: Temperature distribution across spherical vessel's wall

The thermal, mechanical and overall radial stresses computed by using the proposed analytical solution complied well with the FEM result which can be seen in Figure 4.7. Similar to the case of cylindrical pressure vessel, the spherical vessel's wall is under compressive stress because the inner wall is subjected to higher pressure and temperature.

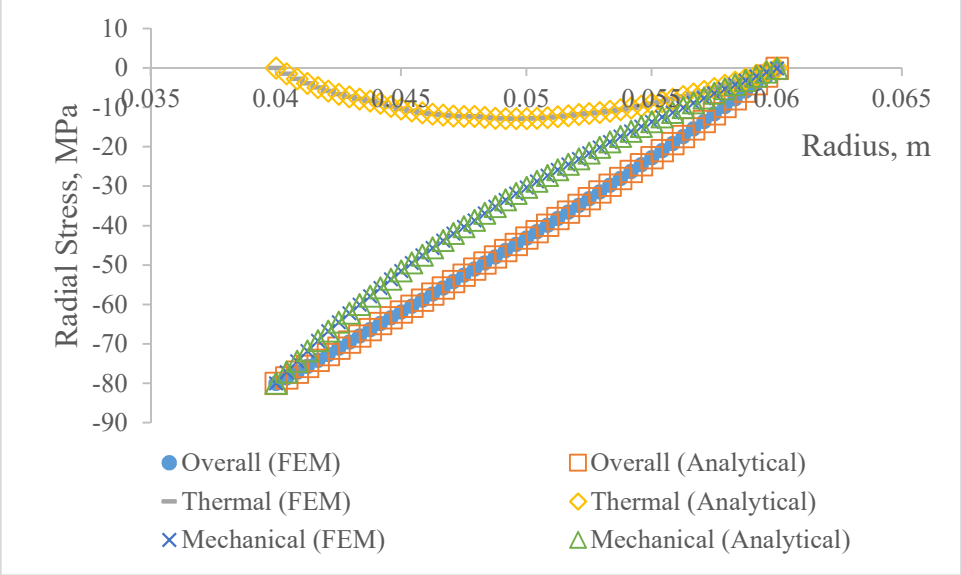

Figure 4.7: Radial stress across spherical vessel's wall

Figure 4.8 shows that the tangential stress obtained by using the proposed analytical solution and FEM is indistinguishable. Tangential stress discontinuities can be observed at interface of layers. In spherical case, tangential stress induced by mechanical loading exhibited an obvious discontinuity pattern at interface point and its trend is in a reversed direction as compared to tangential stress induced by thermal loading. Therefore, the resultant tangential stress shows a smoother transition as compared to cylindrical pressure vessel.

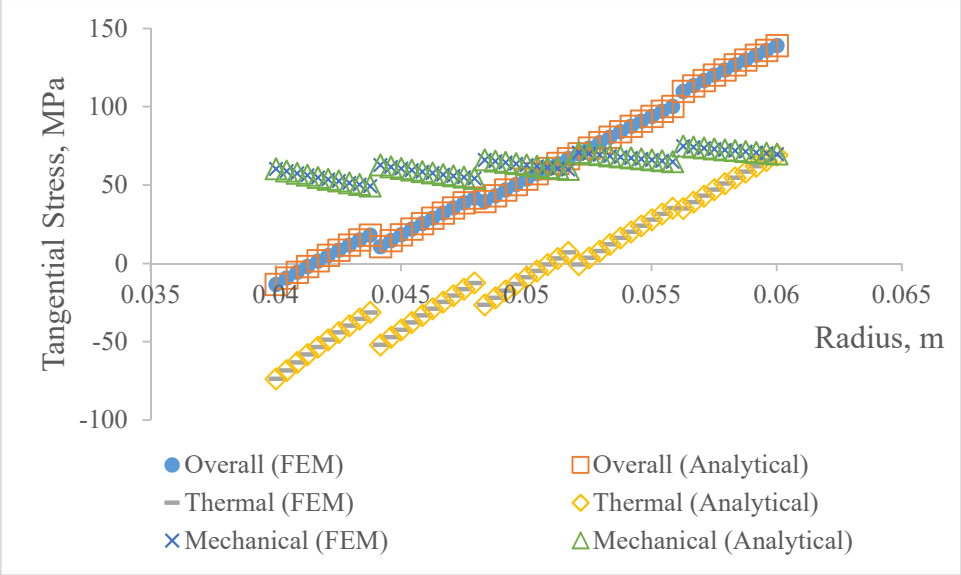

Figure 4.8: Tangential stress across spherical vessel's wall

4.2. Alternative Solution to Solve FGM Problem

Functionally graded material (FGM) is an improved composite material that can eliminate stress discontinuity in layered construction (Toudehdehghan and Hong, 2019). Theoretically, functional graded material properties vary continuously from one surface to other. In this section, both FGM cylindrical and spherical structure was approximated by partitioning the structure into 200 layers. The 200 layers' model is solved by using recursive algorithm and the results are compared with published analytical solution in literature.

4.2.1. Alternative Solution to Solve Cylindrical FGM Problem

Wang et al. (2015) published a work that gave analytical solution for steel cylindrical pressure vessel where the inner surface is coated by power law graded material. The model was used as a benchmark to investigate the

feasibility of the recursive algorithm as an approximation to analytical solution of FGM cylindrical structure under thermomechanical loading. The inner radius of FGM coating is 0.8 m, the outer radius of FGM coating is 0.808 m and outer radius of steel layer is 0.824 m. The material properties are shown in Table 4.3. The internal pressure and temperature are 10 MPa and 120 °C. The external pressure and temperature are 0 Pa and 20 °C. The percentage of differences between results generated by the proposed analytical solution and Wang et al. (2015)'s work are rounded up to 4 decimal places and can be calculated based on $\Omega_z = \left|\frac{z - z_{wang}}{z_{wang}}\right| \times 100\%$ where z can be ${\sigma_{rr}}/{P_{int}}$, ${\sigma_{\phi\phi}}/{P_{int}}$ and ${\sigma_{zz}}/{P_{int}}$.

Table 4.3: Material properties of the cylindrical FGM model

Properties	Inner radius of FGM	Outer radius of FGM	Outer radius of steel layer
E, Pa	2.10×10^{11}	1.90×10^{11}	1.90×10^{11}
$\alpha, °C^{-1}$	19.5	17.25	17.25
$k, Wm^{-1}°C^{-1}$	10.03	45.2	45.2
v	0.3	0.3	0.3

As shown in Table 4.4, the highest percentage of difference recorded is at axial stress for point approaching the outer layer of the FGM coating or inner layer of the steel body which is 0.2059%. Generally, the percentage of difference recorded for all is less than 1%. Therefore, it justified the reliability of using the proposed recursive algorithm to estimate the stress response of FGM cylindrical pressure vessel.

Table 4.4: Result comparison of proposed analytical solution with FGM analytical solution reported in Wang et al. (2015)'s work

r/r_0	σ_{rr}/P_{int}			$\sigma_{\phi\phi}/P_{int}$			σ_{zz}/P_{int}		
	Wang	Present work*	Ω (%)	Wang	Present work*	Ω (%)	Wang	Present work*	Ω (%)
1	-1	-1	0	-2.3824	-2.3865	0.1735	-21.3091	-21.3077	0.0065
1.0025	-0.9839	-0.9843	0.0413	11.7647	11.7510	0.1165	-6.7061	-6.6954	0.1594
1.005	-0.9399	-0.9407	0.0750	20.8824	20.8830	0.0031	2.9307	2.9368	0.2059
1.0075	-0.8781	-0.8787	0.0671	26.6471	26.6796	0.1223	9.2568	9.2465	0.1110
1.01	-0.8053	-0.8056	0.0397	30.2353	30.2707	0.1172	13.3361	13.3299	0.0467
1.02	-0.4502	-0.4501	0.0219	40.7059	40.7055	0.0009	24.1554	24.1252	0.1250
1.03	0	0	0	51	50.9397	0.1183	34.8564	34.8091	0.1357

*Present work based on proposed analytical solution with 201 layers

4.2.2. Alternative Solution to Solve Spherical FGM Problem

In this section, a power-law graded FGM model with the power law index $\beta = 1$ from Bayat et al. (2012)'s work was chosen as the benchmarking results to investigate the feasibility of the recursive algorithm as an approximation to analytical solution of FGM spherical structure under thermo-mechanical loading. The inner and outer radius of the sphere is 0.04 m and 0.06 m respectively, the inner surface elastic modulus and thermal expansion coefficient are $E_{in} = 200\ GPa$ and $\alpha_{in} = 1.2 \times 10^{-6}\ ℃^{-1}$. The power law index is $\beta = 1$. The internal pressure and temperature are 80 MPa and 300 °C respectively while the external pressure and temperature are 0 Pa and 25 °C respectively. The percentage of differences between results generated by the proposed analytical solution and Bayat et al. (2012)'s work are rounded up to 4 decimal places and can be calculated based on $\Omega_z = \left|\frac{z - z_{bayat}}{z_{bayat}}\right| \times 100\%$ where

z can be T/T_{int}, σ_{rr}/P_{int} and $\sigma_{\phi\phi}/P_{int}$.

As can be seen from Table 4.5, the only observable percentage difference is stress in tangential direction and it is generally less than 1% where the highest percentage difference computed was at the inner surface of FGM spherical vessel which is 0.6491%.

Table 4.5: Result comparison of proposed analytical solution with FGM analytical solution reported in Bayat et al. (2012)'s work

r/r_0	T/T_{int}			σ_{rr}/P_{int}			$\sigma_{\phi\phi}/P_{int}$		
	Bayat	Present work*	Ω (%)	Bayat	Present work*	Ω (%)	Bayat	Present work*	Ω (%)
1	1	1	0	-1	-1	0	0.1383	0.1374	0.6491
1.0875	0.7452	0.7452	0	-0.8077	-0.8077	0	0.3492	0.3497	0.1433
1.1875	0.5201	0.5201	0	-0.6010	-0.6010	0	0.5955	0.5956	0.0166
1.2875	0.3454	0.3454	0	-0.4034	-0.4034	0	0.8472	0.8469	0.0325
1.3875	0.2071	0.2071	0	-0.2116	-0.2116	0	1.1045	1.1039	0.0552
1.5	0.0833	0.0833	0	0	0	0	1.4008	1.3999	0.0688

*Present work based on proposed analytical solution with 200 layers

CHAPTER 5

CONCLUSIONS AND RECOMMENDATIONS

5.1. Conclusion

The derivation of the analytical solutions based on recursive algorithm to obtain temperature and stresses distribution for multilayered hollow cylindrical and spherical pressure vessel under steady state thermo-mechanical loading have been described in detail. The proposed analytical solutions were verified through comparison with results obtained by using finite element method (FEM) software ANSYS. Firstly, the two-dimensional FEM models adopted from published literatures are constructed. Next, the steady state thermal analysis was conducted followed by structural stress analysis. Generally, the results agreed well to each other. Similar to findings by other researchers, it can be observed that the overall tangential and axial stresses induced within the cylindrical vessel wall recorded a stepwise discontinuous pattern. In this case, it can be seen that tangential and axial stresses discontinuity at layers' interfaces were attributed to the thermal loading on the vessel. Also, a study was conducted and concluded that the consideration of axial strain has significant effect on Von Mises stress of the cylindrical vessel wall.

After that, the validated proposed analytical solutions were used as the alternative solutions to solve cylindrical and spherical functionally graded

material (FGM) problem. In the study, two published FGM models were extracted from literatures and the FGM wall layers were approximated as 200 layers wall. Overall, the computed results have shown less than 1% difference as compared to the published analytical results.

5.2. Recommendation for Future Studies

The assumptions applied throughout the derivation of the analytical solution has limited the application of the analytical solution. Therefore, future studies can be focused on these assumptions to improve the generality of the derived analytical solution. For example, pressure vessel can be subjected to fluctuating load when steam demand of a power plant varies. Thus, recursive algorithm should also be used to derive the analytical solution for multilayered structure under non-steady state thermo-mechanical loading.

REFERENCES

Abdalla, H. M. A. and Casagrande, D., 2020. Analytical thickness distribution for minimum compliance axisymmetric vessels. *Thin-Walled Structures,* 149**,** pp. 106641.

Akış, T. 2017. On the Yielding of Two-Layer Composite Spherical Pressure Vessels, 2017. Politeknik Dergisi, pp. 9-16.

Alam, S., Yandek, G. R., Lee, R. C. and Mabry, J. M., 2020. Design and development of a filament wound composite overwrapped pressure vessel. *Composites Part C: Open Access,* 2**,** pp. 100045.

ANSYS 2009. Theory Reference for the Mechanical APDL and Mechanical Applications. *In:* Kohnke, P. (ed.). USA: ANSYS Inc.

Arabzadeh, V., Niaki, S. T. A. and Arabzadeh, V., 2018. Construction cost estimation of spherical storage tanks: artificial neural networks and hybrid regression—GA algorithms. *Journal of Industrial Engineering International,* 14**,** pp. 747-756.

Arslan, E., Mack, W. and Apatay, T., 2021. Thermo-mechanically loaded steel/aluminum functionally graded spherical containers and pressure vessels. *International Journal of Pressure Vessels and Piping,* 191**,** pp. 104334.

ASME, 2017. *BPVC Section VIII - Rules for Construction of Pressure Vessels: Division 1.* American Society of Mechanical Engineers.

Babuška, I. and Szabó, B., 2006. On the generalized plane strain problem in thermoelasticity. *Computer Methods in Applied Mechanics and Engineering,* 195**,** pp. 5390-5402.

Bayat, Y., Ghannad, M. and Torabi, H., 2012. Analytical and numerical analysis for the FGM thick sphere under combined pressure and temperature loading. *Archive of Applied Mechanics,* 82**,** pp. 229-242.

Benslimane, A., Medjdoub, C., Methia, M., Khadimallah, M. A. and Hammiche, D., 2021. Investigation of displacement and stress fields in pressurized thick-walled FGM cylinder under uniform magnetic field. *Materials Today: Proceedings,* 36**,** pp. 101-106.

Bergman, E. O. and Calif, A. 1955. ASME Transaction 1955 (Reprint).

Bergman, T. L., Incropera, F. P., DeWitt, D. P. and Lavine, A. S., 2011. *Fundamentals of Heat and Mass Transfer, 7th Ed.* USA: John Wiley & Sons.

Bhavar, V., Kattire, P., Thakare, S., Patil, S. and Singh, R. K. P., 2017. A Review on Functionally Gradient Materials (FGMs) and Their Applications. *IOP Conference Series: Materials Science and Engineering,* 229**,** pp. 012021.

Blass, A., 2016. Symbioses between mathematical logic and computer science. *Annals of Pure and Applied Logic,* 167**,** pp. 868-878.

Boresi, A. P. and Schmidt, R. J., 2009. *Advanced Mechanics of Materials, 6th Ed.* USA: John Wiley & Sons.

Braun 1969. A Review of Piping and Pressure Vessel Code Design Criteria: Technical Report 217. California.

Chattopadhyay, S., 2008. Material selection for a pressure vessel. *ASEE Annual Conference and Exposition, Conference Proceedings***,** pp. 13.869.1-13.869.9.

Chen, W. and Ding, H., 2001. A State-Space-Based Stress Analysis of a Multilayered Spherical Shell With Spherical Isotropy. *Journal of Applied Mechanics,* 68.

Chen, Y. Z. and Lin, X. Y., 2008. Elastic analysis for thick cylinders and spherical pressure vessels made of functionally graded materials. *Computational Materials Science,* 44**,** pp. 581-587.

Cheng, A. H. D., Rencis, J. J. and Abousleiman, Y. Generalized Plane Strain Elasticity Problems WIT Transactions on Modelling and Simulation, 1995. WIT**,** pp. 696.

Delouei, A. A., Emamian, A., Karimnejad, S., Sajjadi, H. and Jing, D., 2020. Two-dimensional analytical solution for temperature distribution in FG hollow spheres: General thermal boundary conditions. *International Communications in Heat and Mass Transfer,* 113**,** pp. 104531.

El-Galy, I., Saleh, B. and Ahmed, M., 2019. Functionally graded materials classifications and development trends from industrial point of view. *SN Applied Sciences,* 1**,** pp. 1378.

Ferreira, F. M. and Martins, A. T., 2009. Recursive Definitions and Fixed-Points. *Electronic Notes in Theoretical Computer Science,* 247**,** pp. 19-37.

Fraldi, M., Esposito, L., Carannante, F., Cutolo, A. and Nunziante, L., 2016. Steady-State Thermoelastic Analytical Solutions for Insulated Pipelines. *Mathematical Problems in Engineering,* 2016**,** pp. 1-13.

Ghajar, A. J. and Cengel, Y. A., 2014. *Heat and Mass Transfer: Fundamentals and Applications, 5th Ed.* New York: McGraw-Hill Education.

Gupta, A. and Talha, M., 2015. Recent development in modeling and analysis of functionally graded materials and structures. *Progress in Aerospace Sciences,* 79**,** pp. 1-14.

Habip, L. M., 1965. A review of recent work on multilayered structures. *International Journal of Mechanical Sciences,* 7**,** pp. 589-593.

Harris, B., 1999. *Engineering Composite Materials.* Institute of Materials: IOM.

Hetnarski, R. B. and Eslami, M. R., 2009. *Thermal Stresses -- Advanced Theory and Applications.* Netherlands: Springer.

Insa, D. and Silva, J., 2015. Automatic transformation of iterative loops into recursive methods. *Information and Software Technology,* 58**,** pp. 95-109.

Khurmi, R. S. and Gupta, J. K., 2005. *Machine Design.* New Delhi: Eurasia Publishing House.

Knowles, N. C., 1984. Finite element analysis. *Computer-Aided Design,* 16**,** pp. 134-140.

Kotousov, A. and Wang, C. H., 2002. Fundamental solutions for the generalised plane strain theory. *International Journal of Engineering Science,* 40**,** pp. 1775-1790.

Lancaster, J. F., 1973. Failures of boilers and pressure vessels: Their causes and prevention. *International Journal of Pressure Vessels and Piping,* 1**,** pp. 155-170.

Lawate, S. and Deshmukh, B. B., 2015. Analysis of Heads of Pressure Vessel. *International Journal of Innovative Research in Science, Engineering and Technology,* 4**,** pp. 759-765.

Li, X., Liu, Z. Y., Li, M. Z., Li, P. L., Zhao, Y. and Wan, S., 2020. Experiments on burst pressure and fragment dispersion effects of small-sized pressure vessel BLEVE. *Fuel,* 277**,** pp. 118145.

Mahamood, R. M. and Akinlabi, E. T. 2017. Types of Functionally Graded Materials and Their Areas of Application. *Functionally Graded Materials.* Cham: Springer**,** pp. 9-21.

Mahdy, W., Kamel, H. and Soaly, E., 2013. Design Improvement of Composite Pressure Vessel Structure. *International Conference on Aerospace Sciences and Aviation Technology,* 15**,** pp. 1-12.

Maleki, M., Farrahi, G. H., Jahromi, B. H. and Hosseinian, E., 2010. Residual stress analysis of autofrettaged thick-walled spherical pressure vessel. *International Journal of Pressure Vessels and Piping,* 87**,** pp. 396-401.

Megyesy, E. F. and Buthod, P., 2008. *Pressure vessel handbook.* Oklahoma: PV Pub.

Mijuca, D. 2006. On dimensional reduction in multiscale, finite element and atomistic, analysis in solid mechanics. *Proceedings of the 2nd WSEAS Int. Conference on Applied and Theoretical Mechanics.* Venice, Italy.

Moss, D. R., 2004. *Pressure Vessel Design Manual, 3rd Ed.* USA: Elsevier Science.

Mukherjee, R., 2019. Reimagining pressure vessels in the 21st century. *Reinforced Plastics,* 63**,** pp. 143-145.

Naik, B. K., Muthukumar, P. and Kumar, P. S., 2018. A novel finite difference model coupled with recursive algorithm for analyzing heat and mass transfer processes in a cross flow dehumidifier/regenerator. *International Journal of Thermal Sciences,* 131**,** pp. 1-13.

Nebe, M., Soriano, A., Braun, C., Middendorf, P. and Walther, F., 2021. Analysis on the mechanical response of composite pressure vessels during internal pressure loading: FE modeling and experimental correlation. *Composites Part B: Engineering,* 212**,** pp. 108550.

Nejad, M., Abedi, M., Lotfian, M. and Ghannad, M., 2016. Exact and Numerical Elastic Analysis for the FGM Thick-Walled Cylindrical Pressure Vessels with Exponentially-Varying Properties. *Archives of Metallurgy and Materials,* 61**,** pp. 1303-1308.

Nikbakht, S., Kamarian, S. and Shakeri, M., 2018. A review on optimization of composite structures Part I: Laminated composites. *Composite Structures,* 195**,** pp. 158-185.

Nikbakht, S., Kamarian, S. and Shakeri, M., 2019. A review on optimization of composite structures Part II: Functionally graded materials. *Composite Structures,* 214**,** pp. 83-102.

Ohji, A. and Haraguchi, M. 2017. Steam turbine cycles and cycle design optimization: The Rankine cycle, thermal power cycles, and IGCC power plants. *In:* Tanuma, T. (ed.) *Advances in Steam Turbines for Modern Power Plants.* Woodhead Publishing**,** pp. 11-40.

Parisher, R. A. and Rhea, R. A. 2012. Chapter 6 - Mechanical Equipment. *In:* Parisher, R. A. and Rhea, R. A. (eds.) *Pipe Drafting and Design (Third Edition).* Boston: Gulf Professional Publishing**,** pp. 112-133.

Perumal, L. and Mon, T. T. 2011. Finite Elements for Engineering Analysis: A Brief Review. *International Conference on Modeling, Simulation and Control.* Singapore: IACSIT Press.

Rao, Y., Kiran, B. and Krishnamohan, R., 2012. Composite Pressure Vessels. *International Journal of Research in Engineering and Technology* 1**,** pp. 597-617.

Reinders, J. E. A., Velthuis, J. F. M. and Spruijt, M. P. N., 2019. Pressure and temperature increase of LPG in a thermally coated pressure vessel exposed to fire: Experimental and model results. *Journal of Loss Prevention in the Process Industries,* 57**,** pp. 55-60.

Rencis, J. J. and Huang, Q. P., 1992. Boundary element formulation for generalized plane strain. *Engineering Analysis with Boundary Elements,* 9**,** pp. 263-271.

Shi, Z. F., Zhang, T. T. and Xiang, H. J., 2007. Exact solutions of heterogeneous elastic hollow cylinders. *Composite Structures,* 79**,** pp. 140-147.

Spence, J. and Nash, D. H., 2004. Milestones in pressure vessel technology. *International Journal of Pressure Vessels and Piping,* 81**,** pp. 89-118.

Thattil, M. and Pany, C., 2017. Design and Analysis of Pressure Vessel with different end domes. International Journal of Science, Engineering and Technology Research, 6, pp. 1225-1233.

Toudehdehghan, A. and Hong, T. W., 2019. A critical review and analysis of pressure vessel structures. *IOP Conference Series: Materials Science and Engineering,* 469**,** pp. 012009.

Vakkilainen, E. K. 2017. 7 - Boiler Mechanical Design. *In:* Vakkilainen, E. K. (ed.) *Steam Generation from Biomass.* Butterworth-Heinemann**,** pp. 167-179.

Vedeld, K. and Sollund, H. A., 2014. Stresses in heated pressurized multi-layer cylinders in generalized plane strain conditions. *International Journal of Pressure Vessels and Piping,* 120-121**,** pp. 27-35.

Wang, Z. W., Zhang, Q., Xia, L. Z. and Hu, D. P., 2012. Exact Solution of Axial Stress for a Multilayered Pressure Vessel Subjected to Mechanical and Thermal Loads. *Applied Mechanics and Materials,* 197**,** pp. 185-189.

Wang, Z. W., Zhang, Q., Xia, L. Z., Wu, J. T. and Liu, P. Q., 2015. Thermomechanical Analysis of Pressure Vessels With Functionally Graded Material Coating. *Journal of Pressure Vessel Technology,* 138**,** pp. 011205(1)-011205(10).

Witolla, T., Sames, P. and Greig, A., 2016. Vessels for the Future. *Transportation Research Procedia,* 14**,** pp. 1641-1648.

Wu, Z. Y. and Li, S. P., 1990. The generalized plane strain problem and its application in three-dimensional stress measurement. *International Journal of Rock Mechanics and Mining Sciences & Geomechanics Abstracts,* 27**,** pp. 43-49.

Yeo, W. H., Purbolaksono, J., Aliabadi, M. H., Ramesh, S. and Liew, H. L., 2017. Exact solution for stresses/displacements in a multilayered hollow cylinder under thermo-mechanical loading. *International Journal of Pressure Vessels and Piping,* 151**,** pp. 45-53.

Zhang, H., Shen, R., Yuan, G., Ba, Z. C. and Hu, Y. F., 2017. Cement sheath integrity analysis of underground gas storage well based on elastoplastic theory. *Journal of Petroleum Science and Engineering,* 159**,** pp. 818-829.

Zhang, H. B., Wang, W. Z., Zhang, S. G. and Zhao, Z. Q., 2018a. Semi-analytic solution of three-dimensional temperature distribution in multilayered materials based on explicit frequency response functions. *International Journal of Heat and Mass Transfer,* 118**,** pp. 208-222.

Zhang, Q., Wang, Z. W., Tang, C. Y., Hu, D. P., Liu, P. Q. and Xia, L. Z., 2012. Analytical solution of the thermo-mechanical stresses in a multilayered composite pressure vessel considering the influence of the closed ends. *International Journal of Pressure Vessels and Piping,* 98**,** pp. 102-110.

Zhang, Z. K., Hui, P. Z., Gu, C. H., Xu, P., Wu, Y. Z. and Hua, Z. L., 2018b. Buckling of cold-stretched cylindrical vessels under external pressure: Experimental and numerical investigation. *Thin-Walled Structures,* 131**,** pp. 475-486.

Zimmerman, R. and Lutz, M. P., 1999. Thermal stress and thermal expansion in a uniformly heated functionally graded cylinder. *J. Therm. Stresses,* 22**,** pp. 88-177.